Summer 8-16-2024

Analysis of Hybrid Hydrogel Scaffolds for Post-bioprinting Density Variation of 3D-printed Chlorella Microalgae Cells

Olubusuyi Ayowole
University of Maine, olubusuyi.ayowole@maine.edu

ANALYSIS OF HYBRID HYDROGEL SCAFFOLDS FOR POST-BIOPRINTING DENSITY VARIATION OF 3D-PRINTED *CHLORELLA* MICROALGAE CELLS

By

Olubusuyi Ayowole

B.Eng., Federal University of Technology Akure, 2009

M.Sc., University of Lagos, 2018

A THESIS

Submitted in Partial Fulfillment of the

Requirements for the Degree of

Master of Science

(in Mechanical Engineering)

The Graduate School

The University of Maine

August 2024

Advisory Committee:

Dr. Bashir Khoda, Associate Professor of Mechanical Engineering, Advisor

Dr. Vincent Caccese, Professor of Mechanical Engineering

Dr. Justin Lapp, Assistant Professor of Mechanical Engineering

ANALYSIS OF HYBRID HYDROGEL SCAFFOLDS FOR POST-BIOPRINTING DENSITY VARIATION OF 3D-PRINTED *CHLORELLA* MICROALGAE CELLS

By Olubusuyi Ayowole

Thesis Advisor: Bashir Khoda

An Abstract of the Thesis Presented
in Partial Fulfillment of the Requirements for the
Degree of Master of Science
(in Mechanical Engineering)
August 2024

Emerging as a beacon of promise, green bioprinting pioneers the fusion of 3D bioprinting technology with the intricate organization of plant cells, particularly microalgae, within engineered tissues. The optimization of this process at an industrial scale hinge upon understanding the post-bioprinting cell growth density variation within hybrid hydrogel biomaterial scaffolds.

This study delves into the convergence of biotechnology and micro-biofabrication, employing a phototropic approach to unravel the behavior of microalgae-based bioinks sequel to their subjection to microextrusion forces during 3D bioprinting. Three hydrogel biomaterials—Alginic acid sodium salt (ALGINATE), Nanofibrillated Cellulose (NFC) – TEMPO, and CarboxyMethyl Cellulose (CMC)—are strategically chosen for their scaffolding capabilities. The investigation unfolds in two folds: the development of bioinks from individual or hybrid hydrogel compositions, and the subsequent analysis of their impact on cell proliferation and morphology. The growth dynamics of *Chlorella* microalgae cells within these varied hydrogel compositions are meticulously probed using periodic absorbance measurements. Additionally, the study examines the shear thinning properties of the hydrogel compositions through viscosity and shear

stress assessments. Notably, NFC demonstrates a reduced shear thinning capacity compared to CMC, as evidenced by viscosity data obtained across various shear strain rates. The results, quantified through absorbance values, unveil intriguing patterns. Mono-hydrogel substrates with pronounced adhesive characteristics tend to curtail *Chlorella* cell proliferation, while Alginate, with comparatively lower adhesion, appears to foster an increase in cell concentration alongside a slight increase in viscosity.

DEDICATION

This work is dedicated to my wife, Abiola Ayowole, for enduring loneliness in support of the advancement of my international career.

ACKNOWLEDGEMENTS

I would like to express my deepest gratitude to my advisor, Dr. Bashir Khoda, for his guidance, support, and valuable insights throughout the entire research process. I extend my thanks to the members of my thesis advisory committee, Dr. Vincent Caccese and Dr. Justin Lapp, for their constructive feedback and valuable suggestions that greatly enhanced the quality of my research.

I am grateful to my family members for providing unwavering support during the highs and lows of my graduate school sojourn. Your love and encouragement have inspired and strengthened me immensely.

A special thank you to my friends, Jane & Tom White-Hassler, Everett Goodwin, Oluwafemi Alaba, Kingsley Fasesin, Ayotunde Olayinka, Shofiqul Islam, Patrick Moroney, Amir Baharvand, Dwight Emerich, and Iyobosa Uwadiae, for their moral support and shared experiences that have made my academic pursuit a significantly enriching experience.

I am grateful to the Office of International Programs, the Graduate School, and the Department of Mechanical Engineering of the University of Maine for providing the necessary resources, facilities, and a conducive academic atmosphere that allowed me to pursue my research with dedication and focus.

This thesis would not have been possible without the collective support of these individuals and institutions. I am sincerely thankful for their contributions to my academic journey.

TABLE OF CONTENTS

LIST OF TABLES

LIST OF FIGURES

LIST OF NOMENCLATURE

A	Area
Abs	Absorbance
ε	Molar absorptivity
η	Viscosity
$\dot{\gamma}$	Shear rate
I	Intensity of light exiting the solution
I_0	Intensity of light entering the solution
K	Shear thinning coefficient
n	Number of moles of absorber
N	Shear thinning coefficient
τ	Shear stress of the substrate
T	Transmittance
u	Flow velocity along the boundary
X	Dimension along which the light travels
y	Height above the boundary

LIST OF ACRONYMS AND ABBREVIATIONS

3D	Three Dimensional
AU	Absorbance Unit
Chl a	Chlorophyll A
Chl b	Chlorophyll B
CMC	Carboxymethyl Cellulose
CNF	Cellulose Nanofibril
ECM	Extracellular Matrix
LED	Light Emitting Diode
NFC	Nanofibrillated Cellulose
OD	Optical Density
UMaine	University of Maine

CHAPTER 1

INTRODUCTION

1.1. Motivation

Green bioprinting, with its vast potential applications ranging from industrial-scale bioplastic production to sustainable biofuel processing techniques, emerges as a field necessitating thorough exploration for the advancement of humanity [1, 2]. The extensive investigation of green bioprinting, particularly in the form of 3D microalgae printing, holds promise across various engineering disciplines and beyond. For instance, it has the potential to revolutionize the production of artificial leaves, photosynthetic skins, and bio-garments, offering sustainable alternatives in architecture and fashion [3]. Moreover, microalgae bioprinting facilitates the development of nutrient-rich food supplements and advanced drug delivery systems, contributing significantly to healthcare advancements [4]. In environmental engineering, microalgae printing presents solutions for wastewater treatment and carbon capture, thus addressing pollution and climate change challenges [5]. Additionally, the application of green bioprinting extends to biosensors for environmental monitoring and diagnostics [6], showcasing the versatility and broad-reaching impact of this technology.

Real-world applications of microalgae, such as the mini t-shirt printed by researchers at the University of Rochester (Figure 1.1) [7], and *Chlorella* supplementation (Figure 1.2), further underscore the significance of microalgae bioprinting [8]. The procedures involved in 3D bioprinting of microalgae offer insights that can advance research towards 3D bioprinting of human tissues and organs, addressing the challenge of organ transplant shortages. Although the origin of this research stems from research based on the 3D bioprinting of blueberry cells, microalgae cells were chosen for preliminary investigation due to their high multiplication rates

and seamless availability compared to the complexity of extracting blueberry stem cells for pre-bioprinting culture. It is believed that results from studies on the bio-printability of microalgae can inform protocols for future 3D bioprinting of other chlorophyll-based plant cells, such as blueberry, which potentially have radiation-preventive properties [9]. Researching the post-3D bioprinting behavior of microalgae bio-constructs, specifically in terms of the variation of algae cell density within different hydrogel compositions, is thus considered a logical and highly impactful step forward.

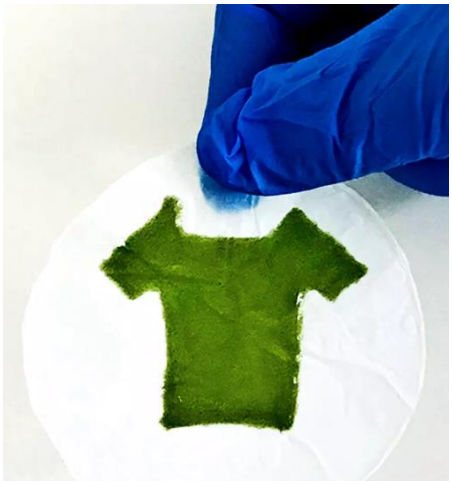

Figure 1.1. T-shirt printed with algae-based ink at the University of Rochester

Figure 1.2. *Chlorella*-based supplement [10]

1.2. Background

1.2.1. Biofabrication Methods

Biofabrication encompasses the automated generation of biologically functional products through the coordinated assembly of living cells, biomaterials, and bioactive molecules via techniques such as bioprinting or bio-assembly [11, 12, 13]. Various methods are employed in biofabrication, including 3D bioprinting, scaffold-based tissue engineering, cell sheet engineering, decellularization and recellularization, microfluidics and organ-on-a-chip, electrospinning, self-assembly and tissue fusion, and biomimicry and bioinspired design [14, 15]. Among these, 3D bioprinting stands out as a potential game-changer, offering an alternative source of organs and reducing reliance on donations from living or deceased individuals [16]. Human organ chip systems, derived from 3D bioprinting, have proven effective in modeling complex diseases and rare genetic disorders [17].

Furthermore, 3D bioprinting presents novel solutions for orthopedic implantation and artificial prosthesis, demonstrating its versatility in the field of medical engineering [18, 19]. Synthetic skin, bioengineered through bioprinting techniques, serves multiple purposes, including assessing the safety and efficacy of pharmaceuticals and cosmetics and providing an ethical alternative to animal testing in scientific research [20]. Organ-on-chips, microscale structures developed by researchers, integrate normal cell culture techniques with microfabrication and microfluidics technology, offering precise models of physiological functions [21].

Decellularization emerges as another vital technique in biofabrication, involving the removal of cellular components from organs or tissues to create a structural extracellular matrix (ECM) template while maintaining a biomimetic microenvironment [22]. This process enables the preservation of native ECM composition and architectural integrity, crucial for tissue

engineering applications [23]. Electrospinning, a technology for producing nanomaterials from polymer nanofibers, finds applications in wound dressings and skin substitutes due to its ability to create interconnected three-dimensional networks [24].

Tissue engineering, employing engineering principles to combine cells, biomaterials, and biochemical cues, aims to restore, maintain, improve, or replace biological tissues [25]. Microfluidic devices, such as organ-on-chips, facilitate the culture of specific cell types within micrometer-sized chambers, enabling the modeling of physiological functions of various tissues or organs under continuous perfusion [26].

1.2.2. 3D Bioprinting and Cell Encapsulation

The evolution of 3D bioprinting has ushered in a new era for tissue engineering and in vitro drug testing. This process, characterized by the layer-by-layer deposition of bioinks using computer algorithms, allows for the creation of intricate 3D structures [27]. Bioprinting, a subset of 3D printing, involves patterning biomaterials to fabricate tissue-like constructs through additive manufacturing technologies [28]. First demonstrated by Klebe in 1988 [29], bioprinting techniques intersect biology and 3D printing by incorporating living cells into a specific medium known as bioink [30].

By utilizing bioinks consisting of cells and other bioactive materials as scaffolds, bioprinting methods enhance the construction of complex tissue structures [31]. However, achieving biocompatibility and printability in tissue scaffold bioprinting can be challenging with a single hydrogel polymer. Combining different materials can address this issue and demonstrate synergistic properties [32]. This advancement in bioprinting holds promise for tissue engineering and regenerative medicine by potentially facilitating model systems for drug screening and

precision medicine applications [33], while also offering precise spatial placement of cells and biologically active particles in tissue formation [34].

The impact of 3D bioprinting extends beyond medicine into the food sector, where it could revolutionize cultured meat production by providing realistic texture, reducing costs, and enhancing ecological sustainability [35, 36, 37]. Moreover, it holds potential in addressing the organ shortage crisis by creating fully functional 3D organs [38], although ethical and legal considerations remain significant hurdles [39]. Figure 1.3 illustrates common techniques of 3D bioprinting, including laser-based, inkjet-based, and micro-extrusion methods [40], with this project adopting the micro-extrusion technique.

Among other factors that contribute to the 3D bioprinting process (Figure 1.4), green bioink formulations play a crucial role in enhancing printability and optimization while adhering to additive manufacturing design principles.

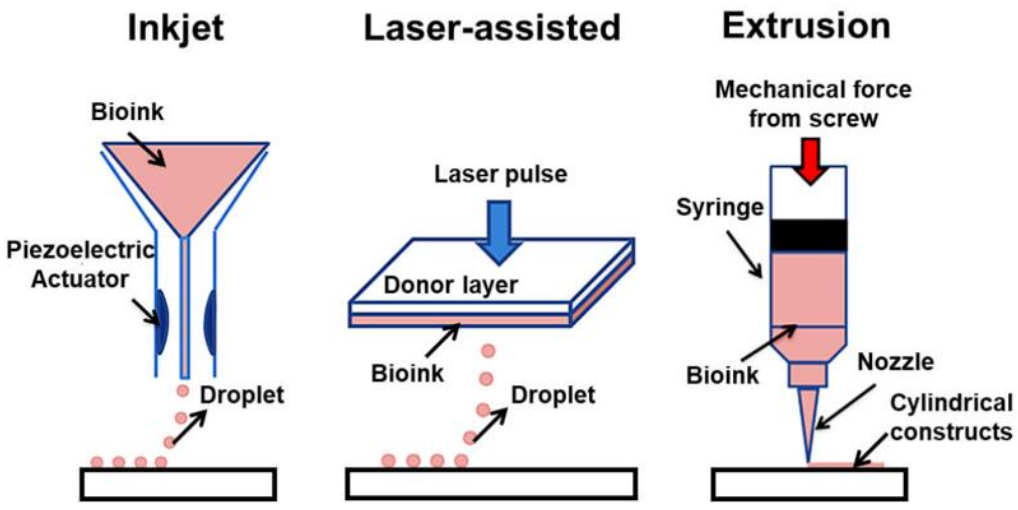

Figure 1.3. Techniques of 3D bioprinting [44]

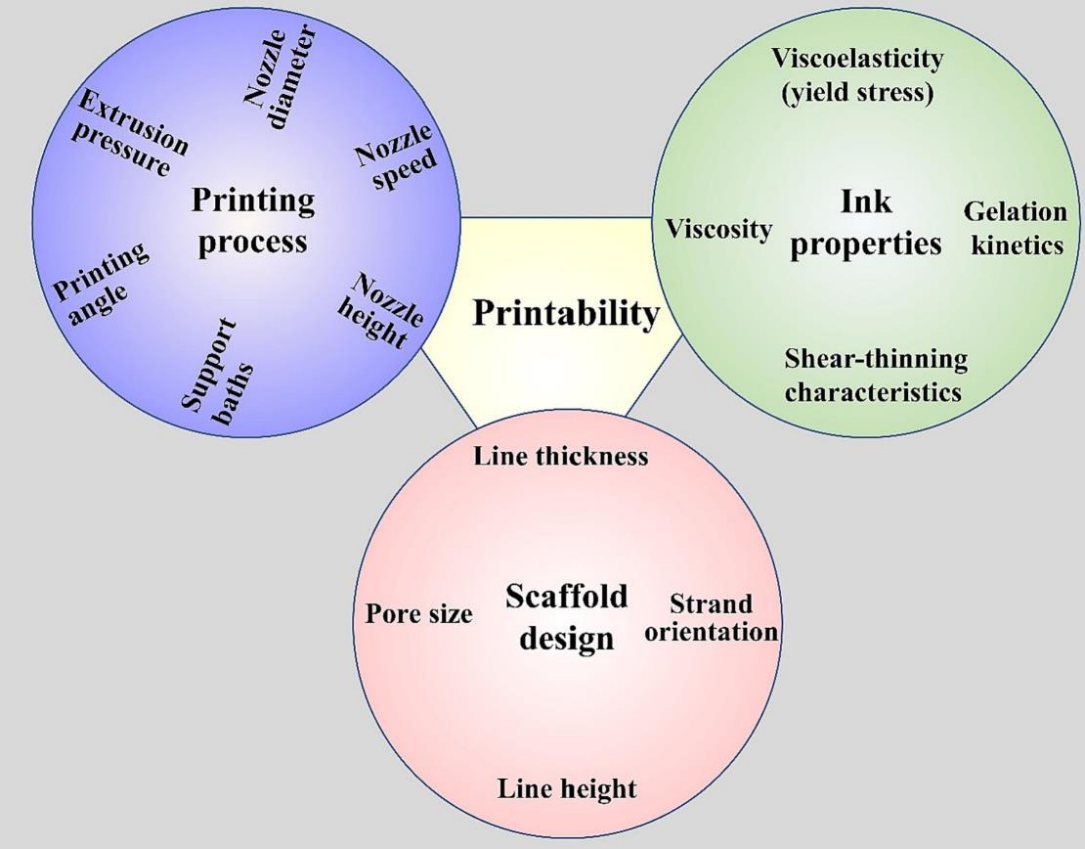

Figure 1.4. Schematic of variables that affect the printability of a bioink [1]

Notably, despite its potential, there are limitations in 3D bioprinting technology, including the high costs associated with bioprinting living cells and in-vitro cell culture [41]. There is also the need for further research into bioinks suitable for cell growth and differentiation [42].

Figure 1.5 showcases some of the top bioprinting systems that have significantly impacted tissue engineering research [43].

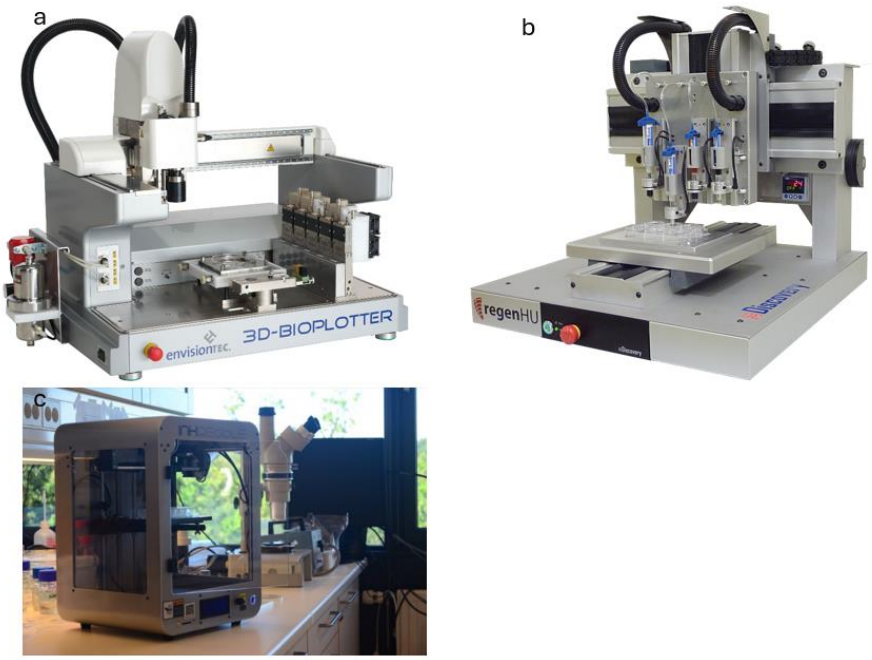

Figure 1.5. EnvisionTEC's 3D bioplotter System (a), RegenHU bioprinter (b), and CELLINK INKREDIBLE 3D bioprinter (c)

Table 1.1. Description, advantages, and disadvantages of different bioprinting techniques

Current Bioprinting Techniques			References
Inkjet bioprinting: Layer-by-layer drop-based deposition of material-cell suspensions driven by pressure pulses. .	Advantages	Low printing cost Fast printing. Relatively high printing precision Reduced risk of contamination	[45]
	Disadvantages	Only suitable for bioinks with low viscosity Difficult to achieve homogenous printing due to clogging tendencies. Liable to rapid drying of the printed construct. This is detrimental to cell survival.	

Table 1.1. (Continued)

Current Bioprinting Techniques			References
Laser bioprinting: Crosslinking of polymer with the aid of light beam. Methods in this category include stereolithography as well as two-photon polymerization.	Advantages	Possible to print bioinks with high cell densities up to 108 cells/mL High bioprinting resolution. Allows a wide range of bioink viscosity. There is no clogging of the bioink.	[46]
	Disadvantages	Relatively time-consuming Higher cost of printing Photon initiators can be toxic to cells	
Micro-extrusion bioprinting: Layer-by-layer deposition of material-cell suspensions onto a predefined location	Advantages	Simple components and control systems. Can print heterogenous constructs. Possible to print high cell densities.	[47]
	Disadvantages	Limited printing resolution and speed Clogging of nozzle tip Mammalian cell viability is often lower than found in models created using inkjet-based bioprinting	

1.2.3. Development of Bioinks

Bioinks are biological materials used in 3D bioprinting for the manufacture of engineered live tissues [48]. The determination of cell types to use and sources of extraction are important in the development of functional bioinks [49]. The biomaterials chosen to form substrates in the bioink are combined with live cells and additives are added to the solution with an aim to model the biological behavior of the components to be bio-printed [50]. It is essential to optimize the bioink composition and printing parameters to ensure the creation of integrated layer-by-layer constructs and functional tissues or organs [51].

Tuning a bioink for biocompatibility, mechanical stability post-printing, and favorable print resolution is paramount in the field of 3D bioprinting [52]. The resolution of each extruded layer, a measure of print resolution, directly influences the quality of the tissue or construct being printed [53]. Moreover, bioinks must not only sustain cell viability but also possess bio-instructive properties to regulate cellular activity and functionality, thus contributing to the successful development of functional tissues [54].

Several factors significantly affect the printability of bioinks, necessitating careful consideration during the formulation process. These factors include viscosity, surface tension, crosslink ability, and the surface properties of the printer nozzle [55]. For instance, a higher gauge nozzle can enhance resolution, thereby improving the fidelity of the printed structures [56]. Additionally, the print speed of the nozzle must be meticulously adjusted to match the flow velocity of the bioink to achieve the desired geometrical characteristics of deposited filaments [57].

Temperature control is another critical aspect of bioink printing as it influences the rheological properties of the bioink and ensures the preservation of cell viability throughout the printing

process [58]. Proper temperature regulation is essential to prevent undesirable changes in bioink viscosity that may compromise print quality or cell integrity.

Furthermore, the extrusion of bioinks must maintain a minimum flow rate to ensure a reasonable print time while avoiding excessive shear stress that could adversely affect cell viability [59]. Achieving the delicate balance between print speed and flow velocity is crucial for the successful deposition of bioinks and the fabrication of functional tissue constructs.

Optimizing bioink formulations and printing parameters is essential for the success of 3D bioprinting endeavors. By fine-tuning these factors, one can enhance print resolution, maintain cell viability, and produce bioinks with bio-instructive properties that regulate cellular behavior. These advancements in bioink technology hold promise for the development of functional tissues and organs, paving the way for innovative solutions in regenerative medicine and tissue engineering [60].

1.2.4. Quantification of Cell Proliferation

Precise quantification of cells in a sample is crucial for effective tissue culture [61, 62]. Various methods exist for quantifying cell count and concentration, including spectrophotometry, flow cytometry, solid phase cytometry, and hemocytometry. Spectrophotometry measures the optical density (OD) at a specific wavelength, albeit indirectly. Flow cytometry, on the other hand, analyzes multiple biological parameters of individual cells or particles within heterogeneous populations. Solid phase cytometry, a newer technique, is particularly useful for detecting and enumerating microorganisms at low concentrations [63].

The hemocytometer, a special microscopic slide consisting of two chambers, offers another means of cell quantification. Each chamber is divided into nine large squares, totaling an area of 1 mm^2. The central counting area, containing 25 large squares, further breaks down into 16 smaller squares (Figure 1.6). Designed for cells ranging in size from 2-30 μm and concentrations of 104-107 cells/mL, the hemocytometer originated from clinical blood analysis but remains widely used due to its affordability [64]. However, its manual counting process is time-consuming, making it inefficient for large-scale analyses. To expedite operations, fully automated systems can handle sample preparation.

Flow cytometry serves not only for cell enumeration but also for detecting membrane, cytoplasmic, and nuclear antigens [65]. Additionally, it aids in drug detection, investigating cell uptake in various chemotherapeutic delivery systems. Meanwhile, spectrophotometry remains a staple for monitoring microbial cell growth, as absorbance correlates with increasing cell density [66]. Fundamentally, spectrophotometry operates on the principle that substances in solution absorb light across specific wavelength ranges (known as absorption spectra), while the remaining light transmits through the sample [67].

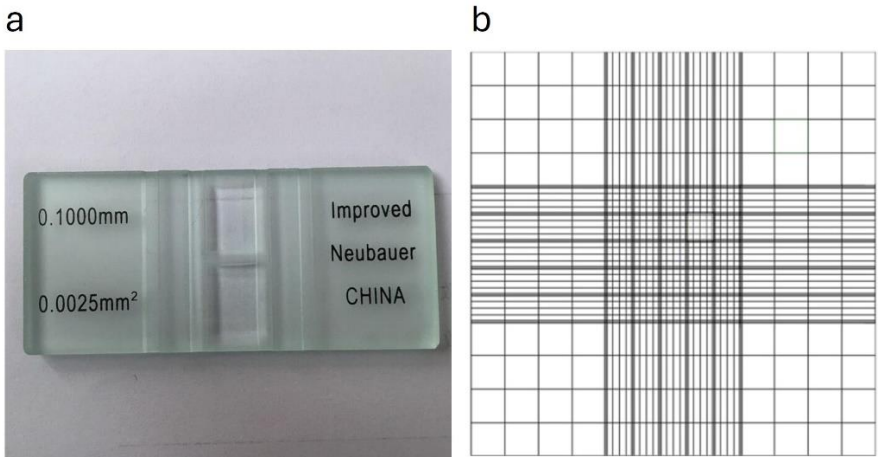

Figure 1.6. Image of a hemocytometer (a), and the Counting grid of a hemocytometer (b)

1.2.5. Controlled Culture of Algae Cells

Various factors significantly influence the biochemical composition of microalgae, including light, temperature, non-mineral nutrients, macronutrients, and micronutrients [68]. Additionally, the pH of the culture media significantly affects microalgae growth, with most species thriving in a pH range of 6–8.76, and some capable of surviving at pH levels of up to 10 [69]. Light intensity also plays a crucial role in regulating the growth and development of algae cells [70].

Continuous monitoring of cell culture is essential for ongoing characterization of cultivated cells [71]. Automation of monitoring and control systems can be effectively implemented in algae photobioreactors, alleviating the need for constant manual measurements and the labor involved in obtaining necessary data during culture [72].

1.2.6. Rheological Characteristics and Printability of Hydrogel Compositions

Hydrogels are biomaterials characterized by three-dimensional (3D) polymer networks with a hydrophilic structure and high-water content, providing an efficient and stable environment for natural tissues [73]. In bioprinting processes, hydrogels offer a biologically relevant microenvironment and exhibit rheological properties necessary to support the printing process [74].

During bioprinting, maintaining an even distribution of cells within the bioink cartridge is crucial. Polymer solutions with low viscosity may struggle to achieve this, leading to cell sedimentation. Studies comparing bioinks with viscosities of 0.003 and 60 Pa·s have demonstrated a significant reduction in cell sedimentation with higher viscosities [75, 76]. However, excessively high viscosity requires higher extrusion pressure, potentially harming cells [77]. Hydrogel viscosity is expected to decrease at high shear rates, with a high shear thinning rate enhancing cell viability and scaffold shape fidelity post-printing [78].

Parameters such as storage modulus, loss modulus, and viscosity are used to predict the printability of bioink formulations [79, 80]. Storage modulus reflects the elastic energy within the bioink, while loss modulus measures the viscous portion or dissipated energy within the bioink [81].

Certain functional hydrogels are sensitive to temperature changes, exhibiting discontinuous changes in shape, appearance, or size over a small temperature range [82]. At any rate, it is essential that hydrogels remain non-toxic [83, 84].

1.3. Research Objectives

The objectives of this study aim to comprehensively investigate cell functionality within 3D bio-printed constructs of algae cells incorporated into hybrid hydrogel scaffold bio-environments. This investigation will be conducted through spectrophotometric analysis, focusing on variations in cell growth density.

Furthermore, the study seeks to identify and establish a set of optimum hybrid hydrogel compositions that are best suited for promoting cell multiplication either before or after subjecting the algae cells-laden bioink to the 3D bioprinting process.

Central to the research are phenomena such as cell proliferation and morphology of microalgae cells, particularly in correlation to the post-printing effects of nozzle wall pressure on cell-laden hybrid hydrogel scaffolds. To achieve this, rheological data of the hydrogel materials will be obtained using a plate-and-cone rheometer to understand their shear thinning properties in relation to cell growth or damage.

Additionally, the study will employ a spectrophotometer to periodically record the absorbance of different compositions of hybrid hydrogel scaffolds. This analysis aims to assess the

survivability and multiplicity of algae cells within each substrate, providing valuable insights into the overall performance and efficacy of the hydrogel scaffolds for cell cultivation and maintenance.

CHAPTER 2

METHODOLOGY

In line with the research objectives, this study primarily investigates the variation in cell density following additive manufacturing of 3D-printed algae cells using scaffolds composed of various hybrid hydrogels.

2.1. Materials

Three bioink scaffolding biomaterials have been adopted for this study to investigate their separate or combined effects on the morphological characteristics of bio-printed *Chlorella* algae cells. They are:

- Alginic Acid Sodium Salt (ALGINATE), sourced from SIGMA-ALDRICH, Co., St. Louis, MO, USA, this material is derived from brown algae.
- Nanofibrillated Cellulose (NFC) – TEMPO, obtained from the University of Maine Process Development Center, Orono, ME, USA.
- Medium Viscosity CarboxyMethyl Cellulose (CMC), also sourced from SIGMA-ALDRICH, Co., St. Louis, MO, USA.

The choice of these biomaterials is inspired by their ability to enhance the functionality of bioinks. Individual characteristics of the adopted scaffolding biomaterials are discussed in subsequent sections of this chapter.

2.1.1. Alginic Acid

Alginates are natural polysaccharide polymers isolated from brown seaweed, extracted using a dilute alkaline solution to solubilize the alginic acid present in the seaweed. When cells are mixed with an alginate-based bioink before printing, the resulting construct provides a suitable microenvironment for cell proliferation. Alginate also exhibits shear-thinning behavior,

facilitating the extrusion process during 3D bioprinting and helping maintain the shape of the printed structure. Alginic acid is a linear polymer (Figure 2.1) composed of D-mannuronic acid and L-guluronic acid residues arranged in blocks within the polymer chain [85]. A sample of Alginic acid sodium salt used in this study is shown in Figure 2.2.

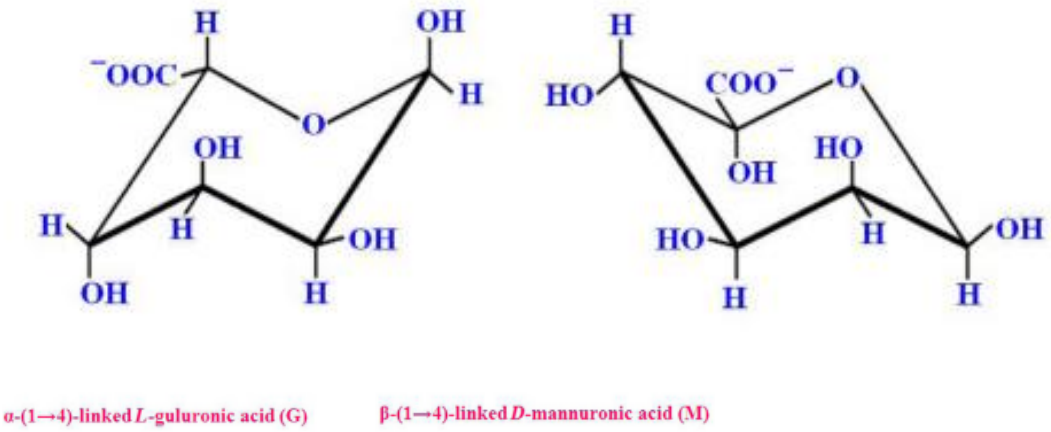

Figure 2.1. Molecular structure of alginate comprising of two copolymeric blocks α-(1-4)-linked L guluronic acid (G), left, and β-(1-4)-linked D-mannuronic acid (M), right [86]

Figure 2.2. Alginate sample

2.1.2. Nanofibrillated Cellulose

Nanofibrillated Cellulose (NFC), also known as Cellulose Nanofibril (CNF), possesses superior properties such as a large specific surface area, high stiffness, high strength, low weight, high biocompatibility, and easy film-forming capability [87]. NFC is extracted using a combination of mechanical and chemical processes to break down cellulose fibers into nanoscale fibrils. Cellulose consists of β-D-glucopyranose units connected by β-1-4-linkages (Figure 2.3), with the basic repeating unit named glucose, and the degree of polymerization (DP) of cellulose varies from several hundreds to over ten thousand [88]. Nanocellulose refers to cellulose with at least one dimension (length, diameter, or height) at the nanoscale [89]. A sample of Nanofibrillated Cellulose used in this study is shown in Figure 2.4.

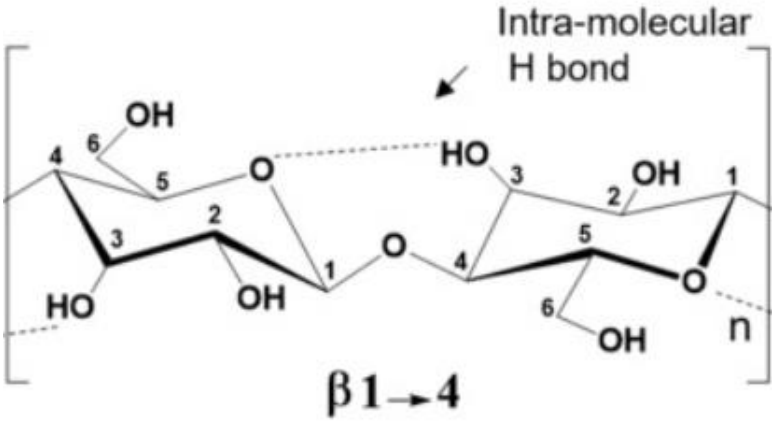

Figure 2.3. Schematic of cellulose repeating unit with the β-(1,4)-glycosidic linkage, intramolecular hydrogen bond is indicated by the dotted lines [90]

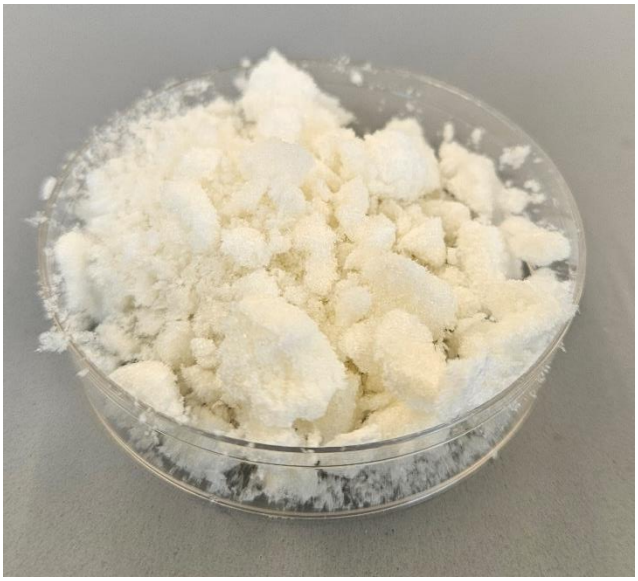

Figure 2.4. NFC sample

2.1.3. Carboxymethyl Cellulose

Carboxymethyl Cellulose (CMC) is a water-soluble derivative of cellulose and a major type of cellulose ether prepared by the chemical attack of alkylating reagents on the activated non-crystalline regions of cellulose. As depicted in Figure 2.5, applications of CMC cut across different areas including tissue engineering, 3D bioprinting, drug delivery, cosmetic fillers, and cancer therapy [91]. CMC is derived by modifying cellulose through the introduction of carboxymethyl groups onto the cellulose backbone (as illustrated in Figure 2.6). CMC stands out as a promising scaffold biomaterial for 3D bioprinting of plant tissues owing to its ease of chemical modification, flexibility, stability, and pH sensitivity. These attributes collectively facilitate the replication of intricate plant tissue structures and functions in engineered constructs, underscoring CMC's suitability for advancing bioprinting technology in the realm of plant tissue engineering. A sample of CarboxyMethyl Cellulose used in this study is shown in Figure 2.7.

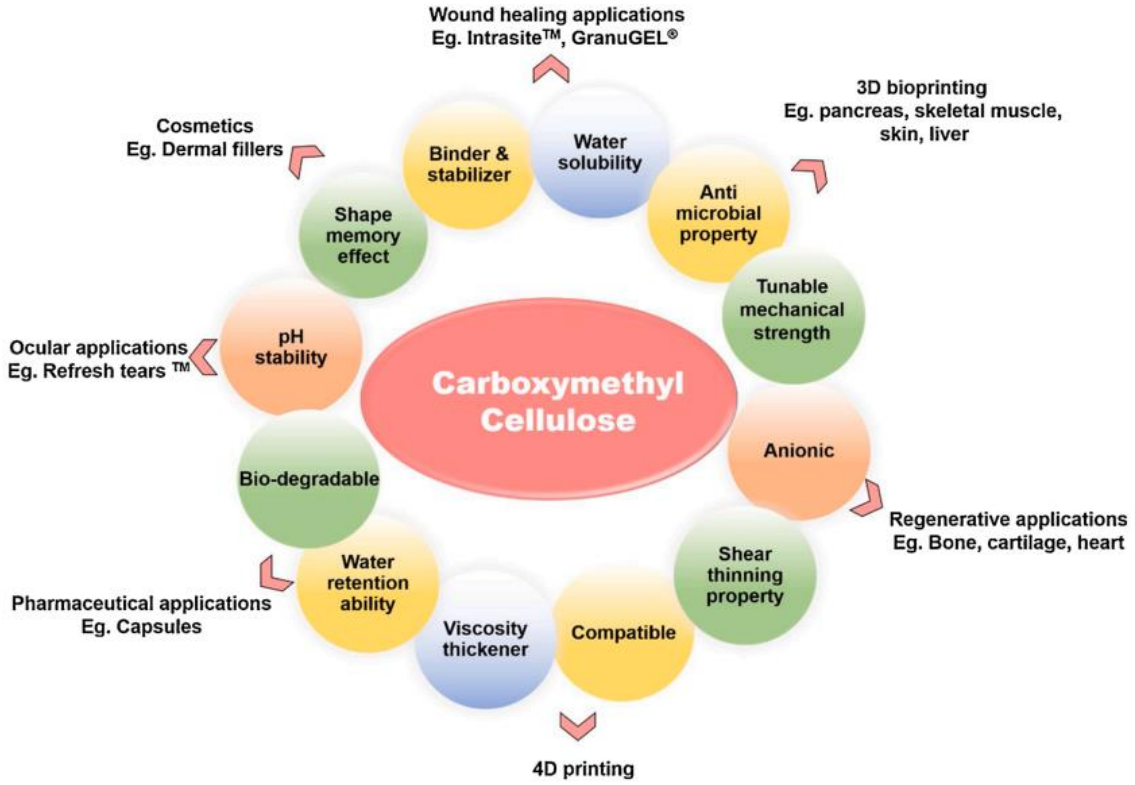

Figure 2.5. Properties and biomedical applications of carboxymethyl cellulose

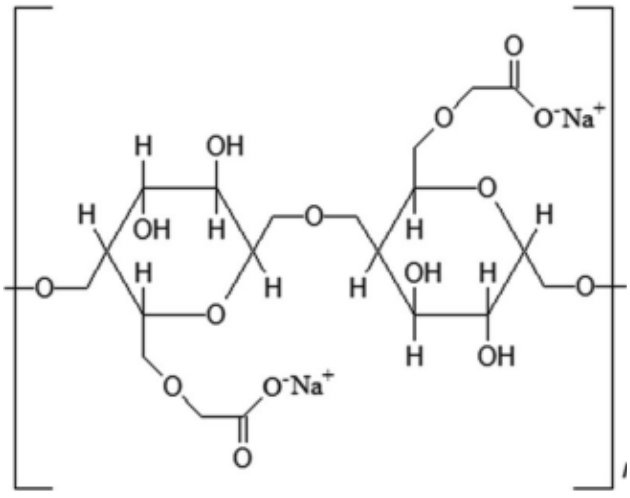

Figure 2.6. Molecular structure of CMC [92]

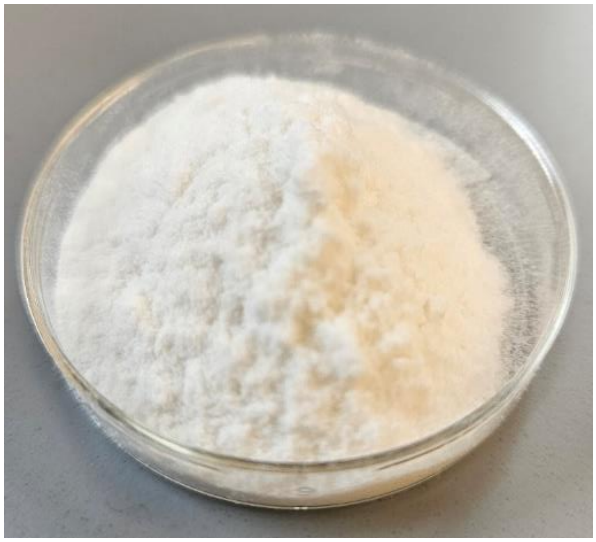

Figure 2.7. CMC sample

2.2. Procedures and Protocols

2.2.1. Sterile Condition Testing

Hydrogel samples were prepared to conduct a preliminary study of their susceptibility to bacterial infection. The biomaterials used in preparing the hydrogels were ALGINATE - Alginic acid sodium salt from brown algae (SIGMA-ALDRICH, Co., St. Louis, MO, USA); NFC - Cellulose Nanofibrils – TEMPO (University of Maine Process Development Center, Orono, ME, USA); and CMC - medium viscosity CarboxyMethyl Cellulose (SIGMA-ALDRICH, Co., St. Louis, MO, USA). A 1% w/v solution of each of the three materials was dissolved using deionized water. The solution of each sample was mixed with a magnetic stirrer hot plate M10102003 (FOUR E's Scientific Co., Guangzhou, China) for 12 hours at 23°C, and the samples were stored in well plates to study the vulnerability of the hydrogels to bacterial infections. The absence of visible black spots on the samples partially suggests an absence of bacterial infection.

2.2.2. Preliminary Preparation of Hydrogel Substrates for Printability Test

The preliminary preparation of hydrogel substrates prior to the set-up of experiments in the study was considered integral towards ensuring the suitability of the hydrogel formulations for 3D bioprinting. This process involves mixing various biomaterials to create hydrogels with homogeneous compositions, suitable viscosities, and optimal printability. Without adequate preparation, the hydrogel may exhibit uneven textures, inconsistent viscosities, or poor compatibility with the bioprinting process, potentially compromising the structural integrity and functionality of the printed constructs.

The mixing of biomaterials was conducted to produce 3D printable hydrogels. To achieve homogeneous mixtures of the biomaterials and distilled water, a digital magnetic stirrer hot plate depicted in Figure 2.8 (Model: M10102003, Manufacturer: FOUR E's Scientific Co., Guangzhou, China) and a magnetic stir bar were utilized.

As earlier mentioned, the biomaterials used to produce the hydrogels were ALGINATE - Alginic acid sodium salt from brown algae (SIGMA-ALDRICH, Co., St. Louis, MO, USA); NFC - Cellulose Nanofibrils – TEMPO (University of Maine Process Development Center, Orono, ME, USA); and CMC - medium viscosity CarboxyMethyl Cellulose (SIGMA-ALDRICH, Co., St. Louis, MO, USA).

A benchmark of 5% w/v composition of biomaterials in deionized water was set, and a series of solutions were produced with ALGINATE, NFC, CMC, and distilled water. Initially, a 5% w/v Alginate solution in 10ml was mixed at 150 rpm and 23°C for 17 hours. Subsequently, a mixture of 3% Alginate and 1% CMC w/v in 10ml was mixed at 150 rpm and 23°C for 17 hours. Following this, a mixture of 3% Alginate and 0.5% NFC w/v in 10ml was mixed at 150 rpm and 23°C for 17 hours.

The choice of mixing speed, temperature, and duration was solely based on the need to achieve a homogeneous mixture.

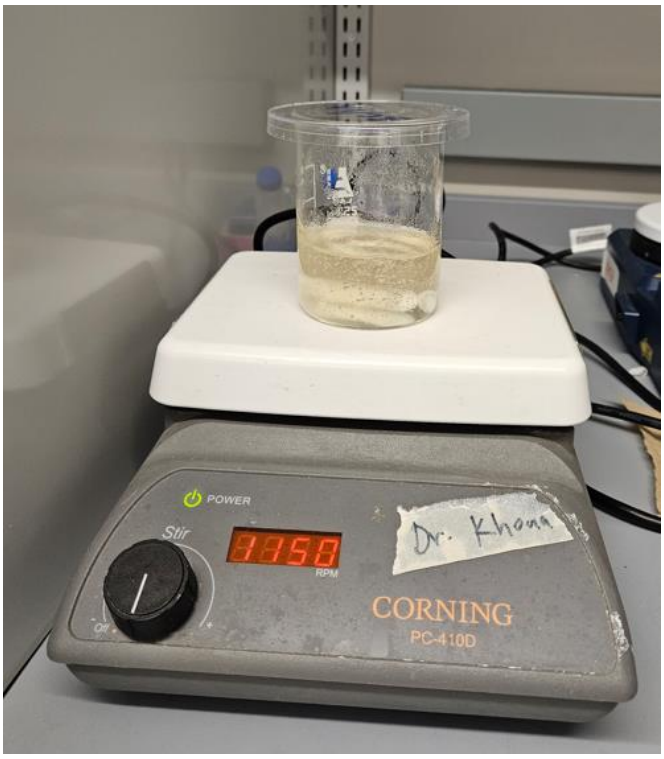

Figure 2.8. Image from the mixing process of hydrogel substrates

To investigate the influence of the angular speed of the magnetic stir bar on the homogeneity of the solution, an increase in speed was examined. Initially, a mixture of 3% Alginate with 0.5% CMC w/v in 10ml at 23°C was stirred at 150 rpm and later at 1100 rpm for 19 hours. Similarly, a mixture of 3% Alginate with 1% NFC and 1% CMC w/v in 10ml at 23°C underwent stirring at 150 rpm and later at 1100 rpm for 19 hours. Additionally, a mixture of 3% Alginate with 1% NFC w/v in 10ml at 23°C was stirred at 150 rpm and later at 1100 rpm for 19 hours. Despite these efforts, limited progress was observed in achieving a homogeneous hydrogel, as NFC dissolved at a slower rate than Alginate and CMC, resulting in a non-uniform texture.

To enhance the homogeneity and viscosity of hydrogels for 3D bioprinting, a strategy involved pre-mixing the NFC component for 24 hours. Specifically, 1% NFC w/v was pre-mixed in 40ml for 24 hours at 23°C and 750 rpm to ensure seamless extrusion and shape fidelity during printing. Some vaporization was noted around the inner part of the film covering the mixing jar. The pre-mixed NFC was then used to initiate solutions containing 2% Alginate, 1% CMC, and 1% NFC w/v in 10ml at 23°C, stirred at 750 rpm and later at 1150 rpm for 46 hours, as well as another solution containing 3% Alginate, 1% CMC, and 1% NFC w/v in 20ml at 23°C, stirred at 750 rpm and later at 1150 rpm for 46 hours. Improved homogeneity was observed in solutions where NFC was pre-mixed longer before combining with Alginate and CMC. This extended pre-mixing facilitated better dissolution of NFC particles, resulting in a more uniform mixture, thereby enhancing overall solution homogeneity and compatibility for subsequent processing in bioprinting applications.

2.2.3. Preparation of Substrates Adopted for Experimental Bioinks

For bioink S1-N1, 1% NFC w/v at 65^{o} C (for the first 45 minutes of stirring) was mixed with 30ml of algae culture medium (ALGA-GRO, CAROLINA BIOLOGICAL SUPPLY, BURLINGTON, NC, USA) for 45 minutes at 450 rpm and for an additional 40 minutes at 1000 rpm. For bioink S1-C2, 2% CMC w/v at 90^{o} C (for the first 30 minutes of stirring) was mixed with 30ml of algae culture medium (ALGA-GRO) for 40 minutes at 750 rpm. For bioink S1-A2:C1, 2% Alginate and 1% CMC w/v at 130^{o} C (for the first 15 minutes of stirring) was mixed with 30ml of algae culture medium (ALGA-GRO) for 30 minutes at 750 rpm. For bioink S1-A2:N1, 2% Alginate and 1% NFC w/v at 95^{o} C (for the first 30 minutes of stirring) was mixed with 30ml of algae culture medium (ALGA-GRO) for 35 minutes at 750 rpm. For bioink S1-A2, 2% Alginate w/v at 65^{o} C (for the first 25 minutes of stirring) was mixed with 30ml of algae

culture medium (ALGA-GRO) for 90 minutes at 1000 rpm. For bioink S1-A1, 1% Alginate w/v at 65^{o} C (for the first 15 minutes of stirring) was mixed with 30ml of algae culture medium (ALGA-GRO) for 15 minutes at 450 rpm and for an additional 85 minutes at 1000 rpm.

For bioink S2-N1:A3, 1% NFC and 3% Alginate (w/v) at 80°C were mixed with 30 ml of the algae culture medium for 40 minutes at 450 rpm, then continued for another 2 hours at 450 rpm and an additional 11 hours at 1000 rpm. For bioink S2-N1:C0.5, 1% NFC and 0.5% CMC (w/v) at 90°C were mixed with 30 ml of the algae culture medium for 40 minutes at 450 rpm, followed by an additional 2 hours at 450 rpm and another 17 hours at 1000 rpm. Similarly, the hydrogel formulation for bioink S2-N1:C0.25 was prepared by mixing 1% NFC and 0.25% CMC (w/v) at 90°C with 30 ml of the algae culture medium for 40 minutes at 450 rpm, followed by an additional 2 hours at 450 rpm and another 17 hours at 1000 rpm. For bioink S2-A3:C0.5:N0.5, an hydrogel formulation was derived with a mixture of 3% Alginate, 0.5% CMC, and 0.5% NFC (w/v) at 90°C stirred with 30 ml of the algae culture medium for 40 minutes at 450 rpm, then continued for another 2 hours at 450 rpm and an additional 10 hours at 1000 rpm. Finally, for bioink S2-A3:C0.25:N0.5 an hydrogel formulations was prepared by mixing 3% Alginate, 0.25% CMC, and 0.5% NFC (w/v) at 90°C with 30 ml of the algae culture medium for 40 minutes at 450 rpm, followed by an additional 2 hours at 450 rpm and another 10 hours at 1000 rpm.

2.2.4. Cell Preparation and Culture

An in-vitro culture of *Chlorella* cells was initiated in an algal medium. This culture was meticulously maintained in a controlled environment, providing optimal conditions for cell growth, including appropriate nutrient concentrations and continuous aeration to facilitate

cellular respiration and metabolism. As the *Chlorella* cells proliferated within the culture medium, they were exposed to sunlight. This step was crucial as it stimulated photosynthesis, a fundamental metabolic process in *Chlorella*, thereby enhancing their metabolic activity and promoting cell health and vitality. Sunlight exposure also served to mimic natural environmental conditions, further priming the cells for subsequent applications.

After the desired growth period, the cultured *Chlorella* cells were carefully harvested from the culture medium. Centrifuging was adopted to isolate the cells while maintaining their integrity and viability. Once harvested, the cells were introduced into the hydrogel substrates to make bioinks. The hydrogel acted as a supportive matrix, providing mechanical stability and spatial organization to the *Chlorella* cells during the bioprinting process.

2.2.5. Preparation of Bioinks

To prepare the initial set of algae cell suspension (Set 1), 0.1 mL of harvested *Chlorella* algae originally from CAROLINA BIOLOGICAL SUPPLY, BURLINGTON, NC, USA, was aliquoted into a 10 mL deionized water in a 15 mL centrifuge tube from FISHER SCIENTIFIC INC., PITTSBURGH, PA, USA. This yielded a cell count of 51.5×10^6 cells/mL with the assistance of a hemocytometer from FRISTADEN LAB, RENO, NV, USA (earlier depicted in Figure 1.6a), and a trinocular LED light microscope shown in Figure 2.9 (M837, OMAX MICROSCOPE, USA) with a 4× lens.

For the preparation of another set of algae cell suspension (Set 2), 0.1 mL of harvested *Chlorella* algae originally from CAROLINA was aliquoted into a 10 mL deionized water in a 15 mL tube from FISHER SCIENTIFIC to obtain a cell count of the pre-cultured algae sample as 55.3×10^6 cells/mL, with the aid of a hemocytometer from FRISTADEN LAB and a trinocular light microscope (OMAX M837) using a 10× lens.

Prior to the estimation of cell count, the hemocytometer was cleaned with 70% ethanol and dried. A cell suspension was prepared and mixed thoroughly. A small volume of the suspension was loaded into the hemocytometer chamber, allowing cells to settle. Using a microscope, cells within a defined grid were counted in multiple squares. The average count was calculated, and concentrations were determined based on the grid size and dilution factor, providing accurate cell counts for this research.

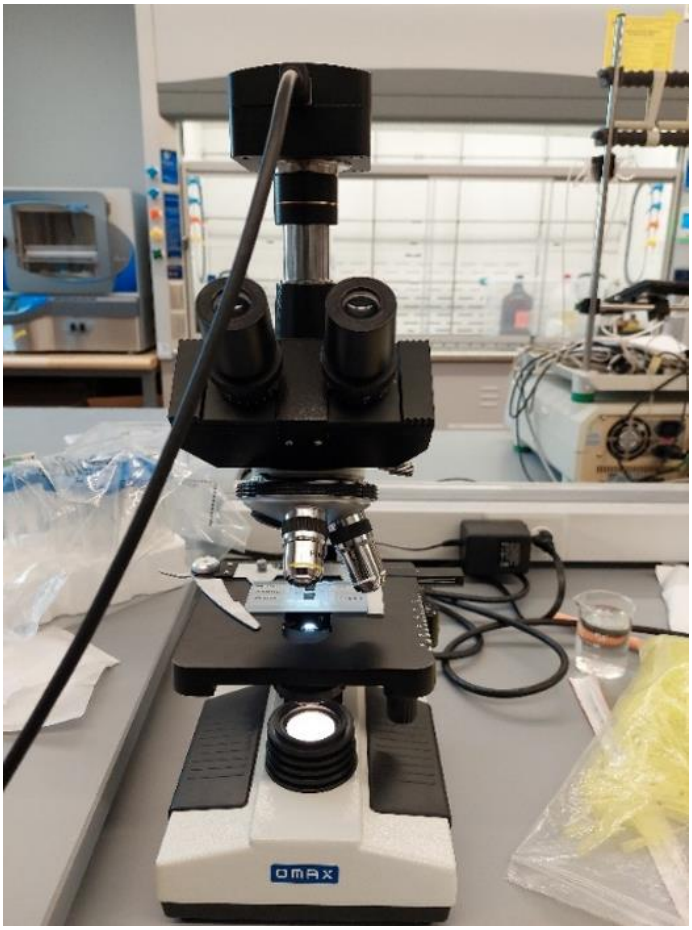

Figure 2.9. OMAX trinocular microscope at UMaine Digital and Additive Manufacturing Lab

Figure 2.10. Centrifuged cell suspension

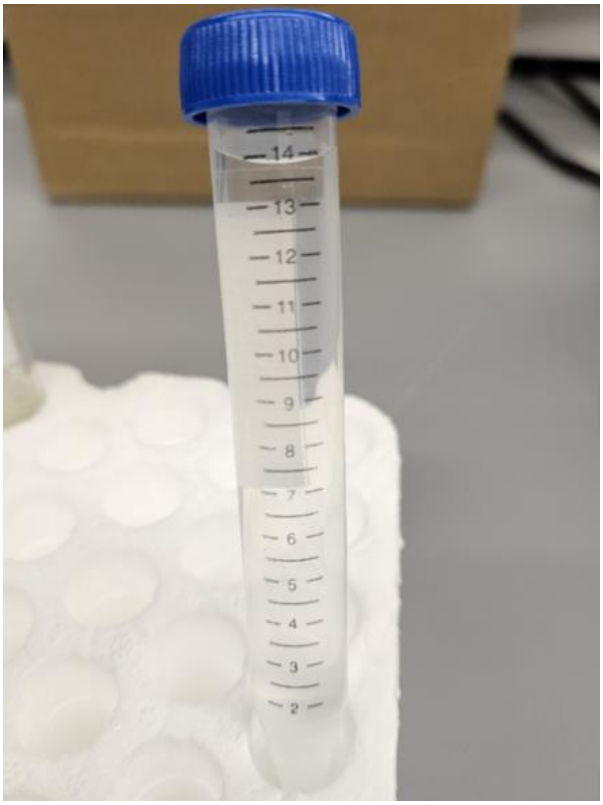

Figure 2.11. Hydrogel substrate in tube before seeding with cell suspension

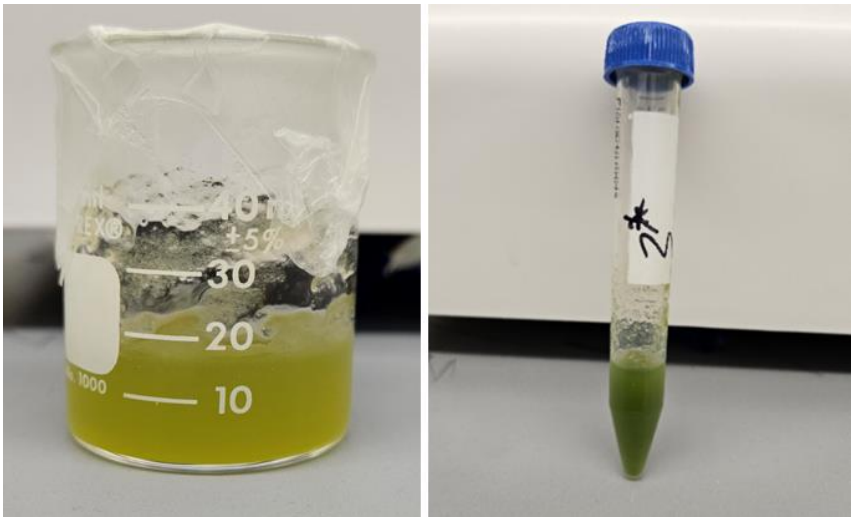

Figure 2.12. Bioinks made up of hydrogel substrates and cell suspensions

An initial set of bioinks was formulated to investigate the impact of extrusion pressure on the post-printing proliferation of *Chlorella* algae cells within each bioink substrate. Bioinks were respectively prepared as S1-N1, S1-C2, S1-A2:C1, S1-A2:N1, S1-A2, and S1-A1 by seeding 0.15 mL of Set 1 cell suspension (51.5×10^6 cells/mL) onto 10 mL of substrates N1, C2, A2:C1, A2:N1, A2, and A1 in a 15 mL tube. For control experiments, 0.15 mL of Set 1 cell suspension was also seeded onto 10 mL of ALGA-GRO media.

To replicate results obtained with bioinks S1-A2 and S1-N1, two samples in a second set of bioinks (S2-A2 and S2-N1) were created. This involved seeding 0.3 mL of Set 2 cell suspension (55.3×10^6 cells/mL) onto 15 mL of substrates A2 and N1. Control experiments in this replication process included seeding 0.3 mL of Set 2 cell suspension onto 15 mL of ALGA-GRO media.

To investigate the effect of nanofibrillated cellulose (NFC) presence in substrates on *Chlorella* algae cell proliferation within microalgae-based bioinks, five additional samples were created in the second set of bioinks. These samples were prepared sequentially by seeding 0.3 mL of Set 2

cell suspension (53.3×10^6 cells/mL) onto 15 mL of substrates N1:C0.5, N1:C0.25, N1:A3, A3:C0.5:N0.5, and A3:C0.25:N0.5 to obtain bioinks S2-N1:C0.5, S2-N1:C0.25, S2-N1:A3, S2-A3:C0.5:N0.5, and S2-A3:C0.25:N0.5, respectively.

Images from laboratory sessions during this study demonstrating the distinction between a cell suspension, hydrogel substrate, and bioink are presented in Figures 2.10, 2.11, and 2.12.

Table 2.1. First set of bioinks (from cell suspension with $51.5 \times 10^6\ cells/mL$)

Bioink	Hydrogel substrate composition	Nomenclature for Substrate
S1-N1	1% NFC	N1
S1-C2	2% CMC	C2
S1-A2:C1	2% Alginate/1% CMC	A2:C1
S1-A2:N1	2% Alginate/1% NFC	A2:N1
S1-A2	2% Alginate	A2
S1-A1	1% Alginate	A1
S1-Media	In Media Only	Media

Table 2.2. Second set of bioinks (from cell suspension with $53.3 \times 10^6\ cells/mL$)

Bioink	Hydrogel substrate composition	Nomenclature for Substrate
S2-A2	2% Alginate	A2
S2-Media	In Media Only	Media
S2-N1	1% NFC	N1
S2-N1:C0.5	1% NFC/0.5% CMC	N1:C0.5
S2-N1:C0.25	1% NFC/0.25% CMC	N1:C0.25
S2-N1:A3	1% NFC/3% Alginate	N1:A3
S2-A3:C0.5:N0.5	3% Alginate/0.5% CMC/0.5% NFC	A3:C0.5:N0.5
S2-A3:C0.25:N0.5	3% Alginate/0.25% CMC/0.5% NFC	A3:C0.25:N0.5

2.2.6. Rheological Properties of Hybrid Substrates

To investigate the effect of extrusion pressure on post-fabrication variations in cell density and morphology, rheological measurements were conducted using a rotational rheometer (ARES-LS2, TA Instruments, New Castle, DE, USA) equipped with parallel plate geometry (20 mm flat

plate). An image of the rheometer used in this study is depicted in Fig. 2.13. The viscosity and shear stress values of the hydrogel substrates were determined by varying the shear strain rate from 1.0 s^{-1} to 100 s^{-1}, with a 0.5 mm gap width set for each measurement at 25°C. The flow characteristic parameters of each hydrogel substrate can be obtained using the Power-Law equation (Eq. 2.1) [93]:

$$\eta = K\dot{\gamma}^{N-1} \quad \text{Eq. 2.1}$$

where η represents viscosity, $\dot{\gamma}$ stands for shear rate, and K and N denote the shear thinning coefficients.

For a Newtonian fluid, the relationship between viscosity and shear stress can be determined by Eq. 2.2.

$$\tau(y) = \eta \frac{\partial u}{\partial y} \quad \text{Eq. 2.2}$$

where τ(y) represents shear stress, u is the flow velocity along the boundary, and y denotes the height above the boundary.

Figure 2.13. Rheometer at UMaine Digital and Additive Manufacturing Lab

2.2.7. Estimation of Cell Growth Rate in Substrates

As indicated in Section 1.2.3, methods suitable for microalgae cell counting include spectrophotometry, hemocytometry, flow cytometry, and solid phase cytometry. In this study, cell counting employs a combination of spectrophotometry and hemocytometry. The steps involved in preparing the cell suspensions used for the study have been outlined in Section 2.2.5.

After formulating the bioinks through the addition of microalgae cell suspension to the hydrogel substrates, cuvettes (ON 67.755, SARSTEDT AG & CO, NUMBRECHT, GERMANY) were filled with 3.7 mL of the bioink samples. Using UV-VIS spectroscopy, the absorbance of each bioink sample was measured with a spectrophotometer shown in Figure 2.14 (721 VISIBLE, NINGBO JUSTOP MEDICAL INSTRUMENTS, NINGBO, CHINA) at wavelengths ranging from 450 nm to 600 nm. It was determined that 450 nm was the most suitable wavelength for absorbance measurements due to the varying transmittance properties of the bioink substrates used in this study.

In this study, the spectrophotometer calibration utilized blank solutions (i.e., the respective hydrogel substrate) in cuvettes matching the refractive properties of those containing the bioink samples. Calibration was enhanced by setting a benchmark absorbance of zero with an empty regular transparent cuvette, and a transmittance of zero with a black cuvette. Calibrations involved parameter setting for absorbance measurement at a predetermined wavelength. Upon insertion of bioink samples contained in cuvettes into the spectrophotometer, measurements of absorbance corresponding to light absorbed by the bioink at the set wavelength, with values recorded for subsequent analysis are obtained. The residual absorbance values were computed by subtracting the absorbance values of the suspension/substrate mixture from those of just the respective hydrogel substrate.

Previous research indicates that the absorption maxima of extracted pigments strongly rely on hydrogel substrate composition and the spectrophotometer type. For deviations exceeding 1 nm, such as in comparative studies with different solutes, absorbance measurement should rely on self-determined maxima rather than conventional values [94]. Studies have also confirmed [95] that Light-harvesting Chlorophylls a and b exhibit absorption peaks between 429 nm and 472 nm, as well as between 642 nm and 674 nm. Based on insights provided from literature, confirmatory spectroscopic experiments were conducted in this study at 650 nm, in addition to measurements obtained at 450 nm, on select bioinks to understand how wavelength choice affects absorbance and cell growth density within the bioinks.

Throughout the study, bioink samples and printed constructs, all contained in cuvettes, were maintained under sterile conditions in a Labanco chemical fume hood, with lighting provided by two pieces of keystone direct drive 2011j LED tubes from the manufacturer. Figure 2.15 illustrates the Labanco chemical fume hood with samples stored using tubes and cuvettes.

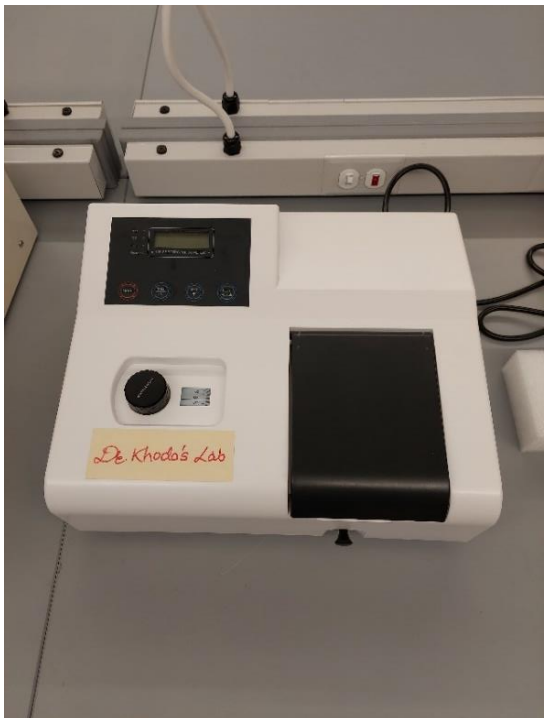

Figure 2.14. Spectrophotometer at UMaine Digital and Additive Manufacturing Lab

Figure 2.15. Labanco hood at UMaine Digital and Additive Manufacturing Lab

Absorbance, a dimensionless measure, is often denoted as AU (arbitrary unit) after its value [96]. Specifying the wavelength of measurement is crucial to avoid ambiguity, as different wavelengths can yield varying absorbance values for a sample. In Figure 2.16, absorption spectra of Chlorophyll a and Chlorophyll b in diethyl ether are depicted, with peak absorbance potentially falling between 400-500 nm and 600-700 nm.

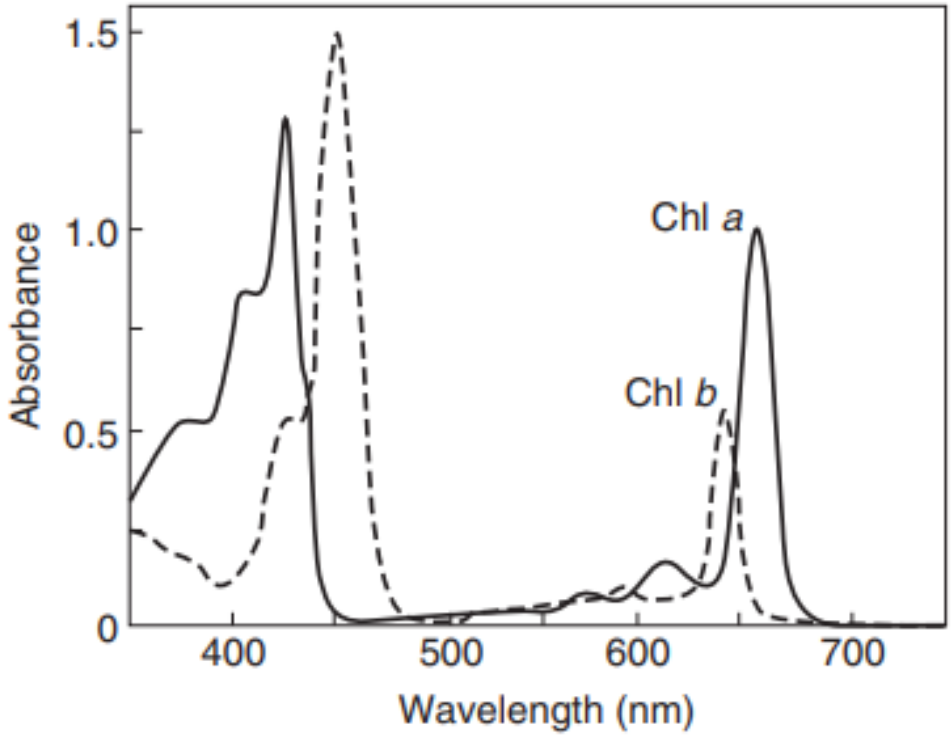

Figure 2.16. Absorption spectra of freshly isolated Chl a and Chl b in diethyl ether [94]

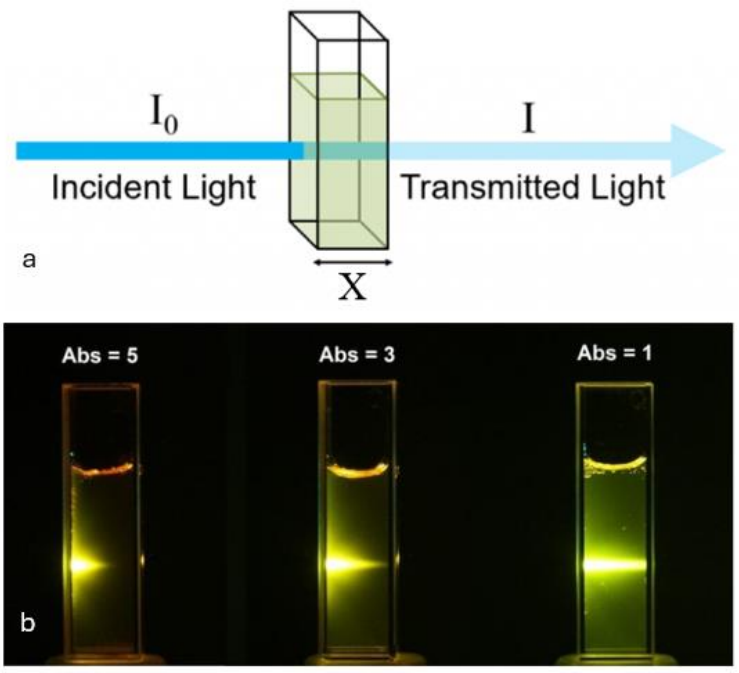

Figure 2.17. Schematic of light transmission through a cuvette (a), Passage of a 510 nm laser through three solutions of Rhodamine 6G with different absorbance values at 510 nm [96] (b)

When a sample of a microalgae-based bioink is confined within a container (like a cuvette) with a path-length X (Figure 2.17a), having walls that are parallel, planar, and non-absorbing at the wavelength of interest, the relationship between the incident light and the transmitted light is established using the Beer–Lambert law, traditionally stated as in Eq 2.3 (a & b):

$$Abs \equiv \ln\left\{\frac{I_0}{I}\right\} = \varepsilon c X \qquad \text{Eq. 2.3a}$$

$$Abs \equiv \frac{\varepsilon n}{S} = \varepsilon X c_{average} \qquad \text{Eq. 2.3b}$$

Where *Abs* is the *absorbance*, I_0 is the intensity of monochromatic light entering the solution perpendicularly to one face and *I* is the intensity of light exiting the solution through the opposite face. The constant ε is known as molar absorptivity with an SI unit of $m^2\ mol^{-1}$. *S* is the cross-sectional area of the cell and *n* is the number of moles of absorber present.

The transmittance *T*, which can be expressed with Eq. 2.4:

$$T \equiv \left\{\frac{I}{I_0}\right\} = \exp\{-\varepsilon c X\} \qquad \text{Eq. 2.4}$$

gives its definition and its interpretation according to the Beer–Lambert law. Eq. 2.5 shows the differential form of Beer–Lambert law which was integrated to obtain Eq.2.3a and Eq.2.3b above.

$$\frac{dI}{dX} = -\varepsilon c I \qquad \text{Eq. 2.5}$$

Where X is the dimension along which the light travels. This differential form of the equation is fundamental, and it is not anchored to any geometry or experiment. Beer-Lambert law primarily links absorbance to concentration and light path length, and it remains unaffected by substrate concentration uniformity. Its robustness stems from several factors. The law assumes homogeneity in the distribution of the absorbing substance across the sample, inherently accommodating concentration variations. Also, its linear relationship ensures absorbance stays

directly proportional to concentration, as long as changes occur uniformly with path length. And, any path length discrepancies due to non-uniformity are automatically corrected by the equation, which explicitly incorporates path length. In essence, Beer-Lambert's law stands as a reliable tool, applicable across various scenarios, even when substrate concentrations within a sample lack perfect uniformity [97].

2.2.8. Printability Test on Hydrogel Constructs

In this study, a custom XYZ-axis micro-extrusion 3D bioprinter (Figure 2.18), specifically developed for biomedical projects at our Additive and Digital Manufacturing Laboratory, is utilized to fabricate experimental constructs using microalgae-laden bioinks under sterile conditions. The bioprinter's dispense assembly (Figure 2.19), featuring a disposable syringe barrel (EFD, Nordson, Westlake, OH, USA) and dispensing tip (EFD, Nordson, Westlake, OH, USA) with an inner diameter of 410 μm, ensures precise dispensing of the bioink onto a stationary print bed. G-Codes are generated using Visual-Basic scripting to create vectorized toolpaths for the bioprinter, ensuring accurate deposition of the bioink. An image of toolpath simulation for the experimental bioprinting undertaken in this project is depicted in Figure 2.20.

The meticulous configuration of the setup, including images of the bioprinter and dispense assembly, enhances comprehension of the experimental bioprinting process. Toolpath simulation aids in optimizing the printing process by visualizing the trajectory of the printing nozzle. These steps collectively enable the assessment of printability, crucial for evaluating the suitability of hydrogel constructs for various applications.

The custom development of the bioprinter underscores its tailored functionality for biomedical research applications, providing a precise and versatile tool for fabricating intricate biological structures. The utilization of industry-standard components, such as the syringe barrel and dispensing tip from EFD (Nordson, Westlake, OH, USA), ensures reliability and compatibility with established protocols and practices in the field of bioprinting.

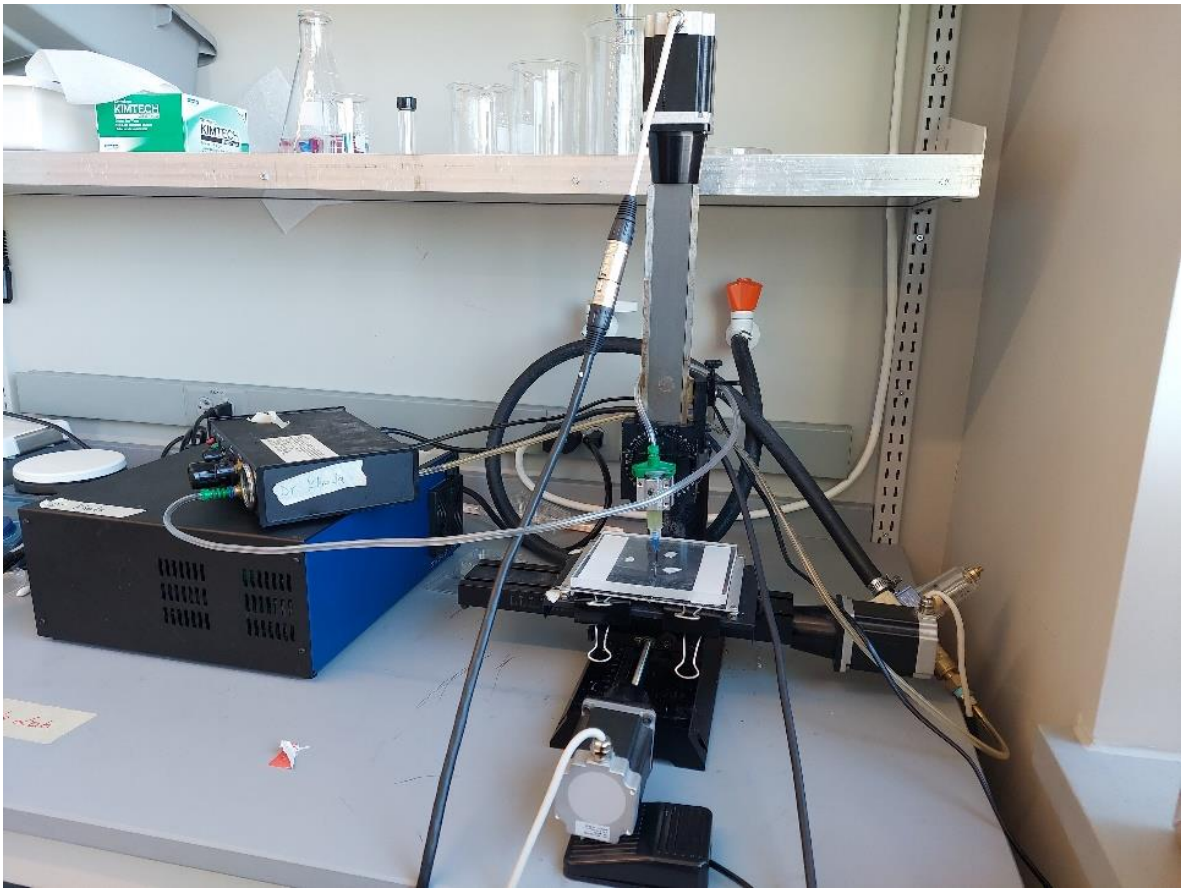

Figure 2.18. 3D bioprinter at UMaine Digital and Additive Manufacturing Lab

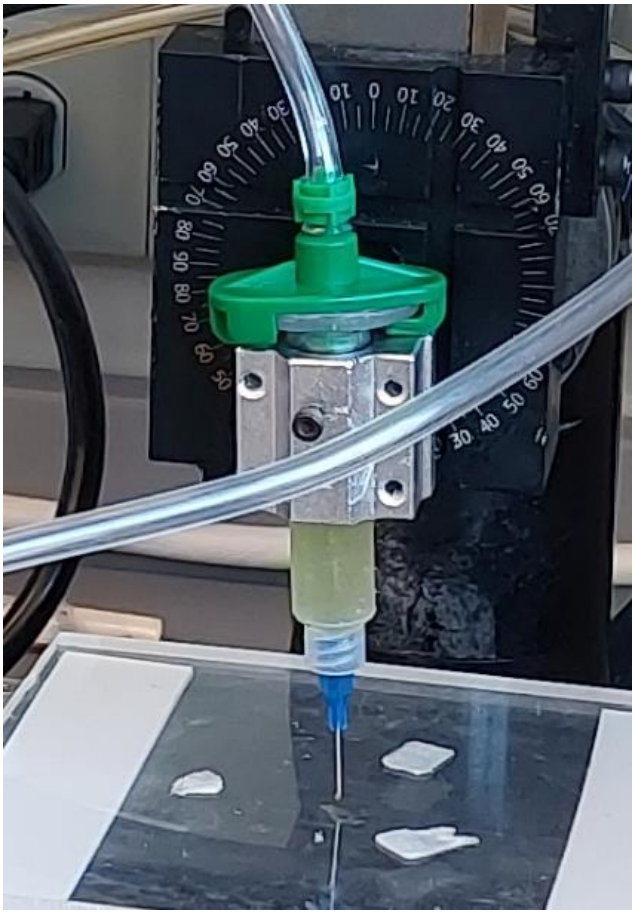

Figure 2.19. Dispense assembly of custom bioprinter at UMaine Digital and Additive Manufacturing Lab

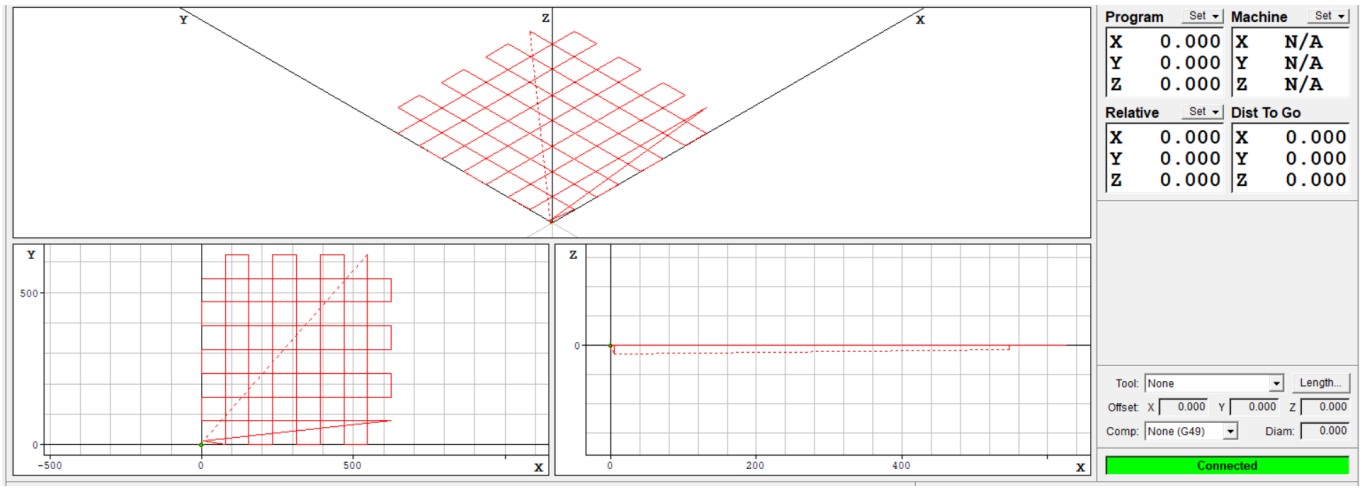

Figure 2.20. Image of toolpath simulation from *Flashcut* controller of the experimental bioprinter at UMaine Digital and Additive Manufacturing Lab

CHAPTER 3

EXPERIMENTAL EVALUATION AND RESULTS

This chapter delves into a comprehensive exploration of various hydrogel compositions to facilitate the rapid proliferation of microalgae cells. It encompasses rheological testing on diverse hydrogel substrates and spectrophotometric analyses of *Chlorella* microalgae-based bioinks. Furthermore, experimental 3D bioprinting of selected microalgae-based bioinks is conducted, with all bioink formulations synthesized as part of the experimental procedures.

Sample images of hydrogel substrates (see Figure 3.1) and microalgae-based bioinks (see Figure 3.2) utilized in the study are presented. The primary objective is to pinpoint the optimal hybrid hydrogel substrate for post-3D-printing culture of *Chlorella* microalgae. Throughout this investigation, the spectrophotometer plays a pivotal role in assessing the efficacy of these compositions.

For a proper demonstration of the results obtained in this research project, a collection of figures and a table essential for understanding the outcomes of the experimental investigation are presented in this chapter. Figure 3.3 offers a comparative analysis of the rheological characteristics of hydrogel substrates, laying the groundwork for understanding their mechanical properties crucial for bioprinting. Microscopic depictions in Figure 3.4 illustrate *Chlorella* cell behavior over multiple days within different substrates, providing visual insights into cellular responses. Figures 3.5 to 3.7 delve into absorbance variations of bioinks, elucidating optical density correlations with cell count and proliferation dynamics. Discrete representations in Figures 3.8 and 3.9 showcase cell density variations in bioinks before and after nozzle tip printing pressure, highlighting pressure's impact on cellular distribution within constructs. Figure 3.10 explores the effect of NFC content on cell density, while Figure 3.11 investigates printing

pressure's influence on cellular outcomes. Calibration curves in Figures 3.12 and 3.13 offer quantitative frameworks for correlating absorbance values with cell counts. Finally, Figures 3.14 and 3.15 provide comparative analyses of bioink rheology and physical properties, crucial for understanding printability and construct integrity. Complementing these figures, Table 3.2 summarizes key physical properties of experimental bioinks and process variables, offering a comprehensive overview of the experimental setup. Together, these visualizations and tabulated data form the foundation for a detailed exploration of the experimental results.

The data collection process involved meticulous procedures to ensure accuracy and reliability. For hydrogel samples cultured via cuvettes without prior passage through the bioprinter, four sets of the same sample were simultaneously prepared and monitored for data collection. Similarly, for samples cultured after subjecting the bioinks to bioprinting, three sets of the same sample were prepared and monitored for data collection, enabling the assessment of any variations introduced by the bioprinting process. In the case of rheological data collection, tests were conducted in duplicate for each hydrogel, cell suspension, or bioink sample, to ensure consistency and accuracy in the measurement of rheological properties. Subsequently, average values for each data point were calculated to generate the respective curves, with error bars incorporated using standard deviation to illustrate variability and provide insights into the reliability of the measurements. This meticulous approach to data collection and analysis ensures the integrity and validity of the findings presented in this study.

This research endeavor is significant for advancing microalgae culture techniques, which hold immense potential across diverse domains such as biotechnology, bioenergy, and environmental remediation. By unraveling the intricate interplay between different hydrogel compositions and microalgae growth, this study offers valuable insights into optimizing culture conditions for

augmented microalgae production. Ultimately, these findings contribute to the development of sustainable solutions for various industrial and environmental challenges.

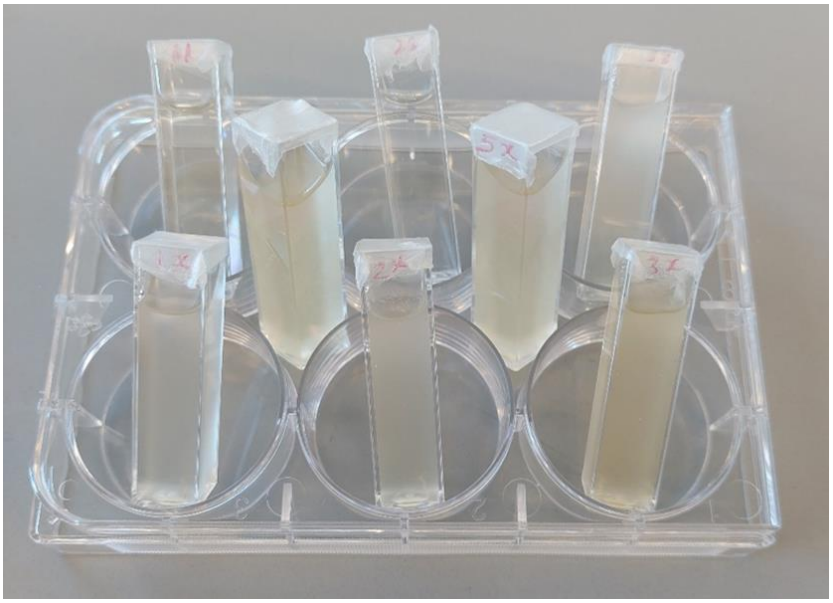

Figure 3.1. Hydrogel substrate samples contained in cuvettes

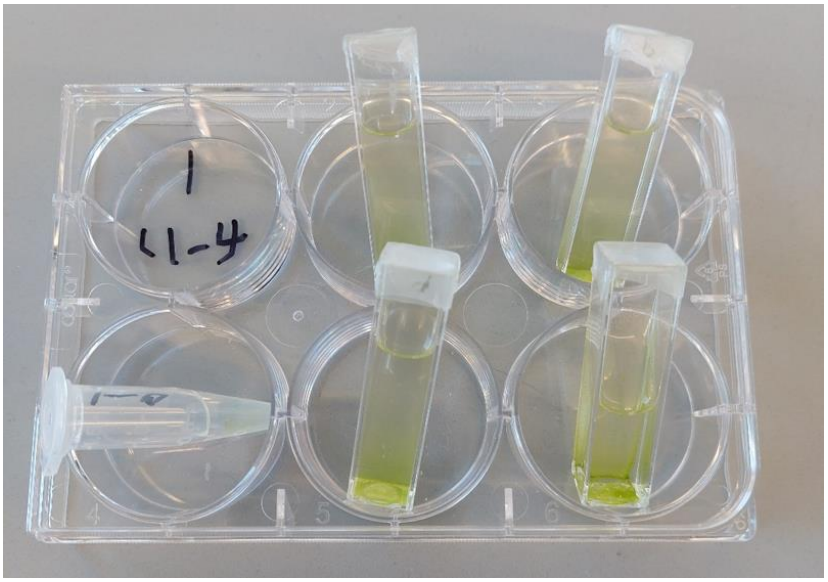

Figure 3.2. *Chlorella*-based bioink samples contained in cuvettes

3.1. Rheology of Hybrid Hydrogel Substrates

To comprehend the influence of viscosity and shear stress on the printability of hybrid hydrogel substrates and their potential to enhance or impede cell proliferation and morphology, shear

stress-shear rate curves for hydrogel compositions are depicted in Figures 3.3. Previous models (Eq. 2.3) from literature have been cited in this thesis to support the systematic approach employed in this study. Shear stress values of hydrogel substrates were determined using a rotational rheometer equipped with a 20 mm parallel plate geometry. The shear strain rate ranged from 1.0 s^{-1} to 100 s^{-1}, with a 0.5 mm gap width for each measurement at 25°C. At a shear rate of approximately 6.31 s^{-1}, the rate of shear stress increase for the 2% Alginate/1% NFC composite began to plateau. This trend persisted until just before reaching a shear rate of about 70.8 s^{-1}, where the 2% Alginate/1% CMC composite exhibited higher shear stress values. This transition indicates a shift in the rheological behavior between the two compositions. Table 3.1 presents an overview of the shear stress values demonstrated by each hydrogel composition during the rheological analysis, specifically focusing on the shear rate of 70.8 s^{-1}. These findings highlight the importance of comprehending the rheological characteristics of diverse hydrogel compositions, as it influences their suitability for bioink formulation in 3D bioprinting.

Table 3.1. Shear stress and viscosity of hydrogel samples at a shear rate of 70.8 s^{-1}

Hydrogel Sample	Shear Stress (Pa) at 70.8 s^{-1}	Viscosity (Pa.s) at 70.8 s^{-1}
2% CMC	160.77	2.27
2% Alginate/1% CMC	90.63	1.28
2% Alginate/1% NFC	87.77	1.24
1% NFC	28.68	0.41
2% Alginate	2.65	0.04
1% Alginate	0.62	0.01

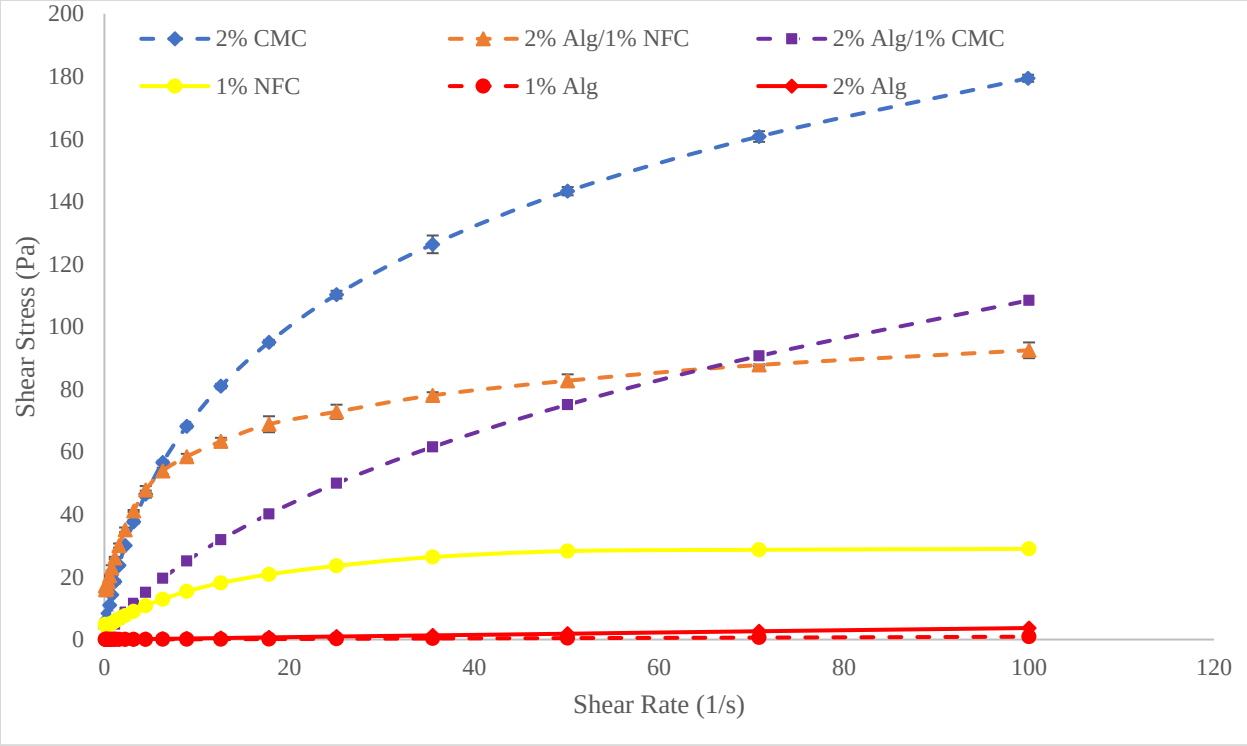

Figure 3.3. Comparison of rheological characteristics of hydrogel substrates

During this study, it was observed that CMC and NFC exhibit superior adhesive properties compared to Alginate. The adhesive capacity of bioinks is crucial for maintaining the precise shape of constructs formed from these materials. It determines the ability of the cell suspension to adhere to the substrate and maintain structural integrity during printing and subsequent processing, thus influencing the fidelity of the final construct. This adhesive property enables the bioink to securely bond to the desired surface and maintain its form, facilitating the fabrication of complex structures with high accuracy and reproducibility in bioprinting applications.

It was observed that due to NFC's significant stickiness even at lower concentrations (1% w/v) compared to CMC (2% w/v), it was challenging to prepare a solution with 2% NFC w/v because its high viscosity hinders stirring and homogeneity attainment. However, investigations revealed that up to 2% CMC w/v could be successfully incorporated into hydrogel substrates to achieve

reasonable homogeneity. The notable increase in shear stress in the 2% Alginate/1% NFC composition compared to solely 1% NFC can be attributed to enhanced crosslinking. The combination of Alginate's gel networks and NFC's reinforcement appeared to result in a stronger, stiffer material with improved cohesion, indicating the significant impact of combining Alginate and NFC.

As will be discussed later in this thesis, it has been confirmed that Alginate exhibits a strong tendency to support the seamless proliferation of cells when added to a hydrogel substrate consisting solely of Alginate and Media. However, while a greater amount of Alginate may enhance cell growth, this study has confirmed a drawback: Alginate alone lacks sufficient viscosity to serve as a standalone substrate for a green bioink without the addition of materials such as NFC and CMC, which possess greater adhesive capacity than Alginate.

It is observed that NFC exhibits lower shear thinning for lower values of shear rate, but it gradually becomes less viscous than CMC with increasing shear rate. At a shear rate of slightly before 70.8 s^{-1}, the solution containing 1% CMC w/v demonstrates superior adhesive capacity compared to the solution with 1% NFC w/v. This difference may stem from CMC's inherent properties, such as its ability to form strong adhesive bonds due to its high molecular weight and hydrophilic nature. In contrast, while NFC offers reinforcement, it may not possess the same adhesive properties, resulting in lower adhesion at this shear rate.

The significant adhesive capacity has been ascertained for the high viscosity hydrogel substrates because they have shown a tendency to remain cohesive for the most part after subjection to the bioprinting process. Analyses have been conducted with the aid of shear stress values because it relates more to viscosity than the mechanical forces involved in the bioprinting process. A direct

correlation exists between shear stress and the viscosity of hydrogel materials. As shear stress increases, viscosity typically follows suit, resulting in a proportional relationship.

This relationship is fundamental in understanding how hydrogel materials respond to external forces, such as shear, and can be crucial in precise control over viscosity during micro-extrusion 3D bioprinting. Understanding and manipulating this relationship allows for the optimization of hydrogel formulations to meet specific performance requirements.

3.2. Spectrophotometric and Morphological Analysis

The approach adopted in this study to quantify the multiplication or elimination of algae cells in hydrogel constructs involves the study of change in cell density or concentration over a period ranging between one day and about 15 days. Absorbance values for the bioink at a wavelength of 450 nm (in most instances) are taken for each bioink on the day of the production of the bioinks, and on select days in-between, till up to 14 days after the production of the bioink. All samples were contained in cuvettes exposed to the same intensity of light in the hood. To investigate the post-3D printing morphology and proliferation of *Chlorella,* an investigation was launched into the best way to capture the variation in the spectroscopic properties of the different hydrogel substrates used for this study, and the curves presented in this section are used for comparative analysis accordingly. The details of the nomenclature adopted for the bioinks used for analysis in this study have been summarized earlier in tables 2.1 and 2.2. Microscope images from the culture of *Chlorella* cells during this study are given in Figure 3.4.

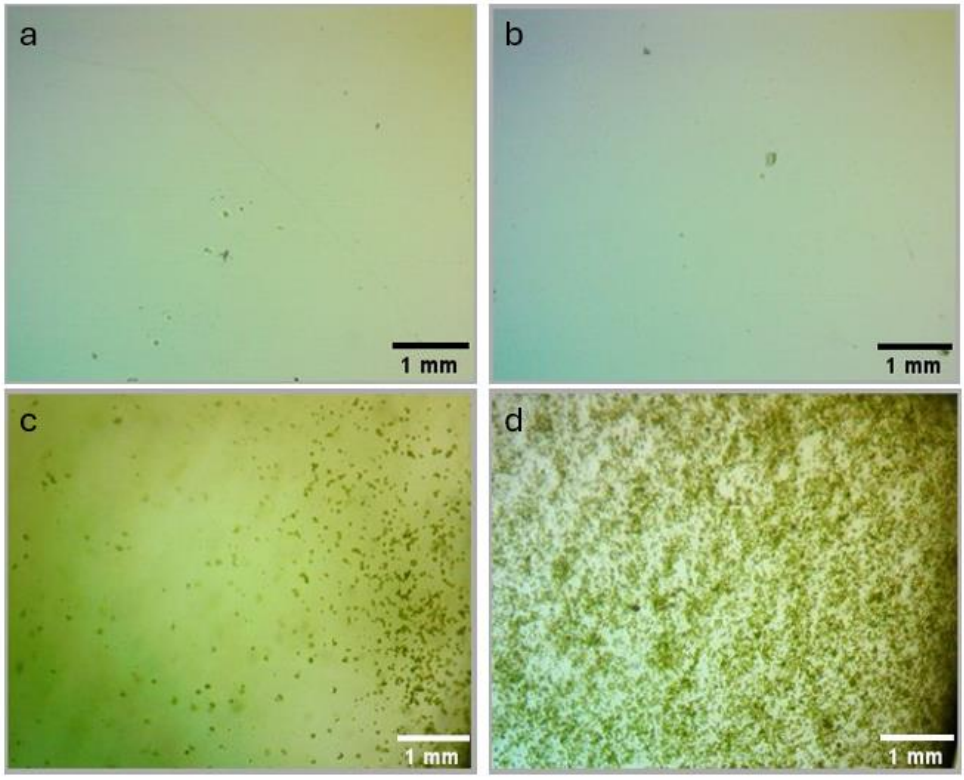

Figure 3.4. Microscopic depiction of *Chlorella* cell behavior: (a) Day one in 1% Alginate; (b) Day two in Media; (c) Day five in 1% Alginate; (d) Day five in Media

Figure 3.5 compares the variation of absorbance for the first set of bioinks over a period of 17 days, and Figures 3.6 and 3.7 contain curves used to replicate bioinks S1-A2, S1-Media, and S1-N1 with bioinks S2-A2, S2-Media, and S2-N1, respectively. Bioinks S2-A2, S2-Media, and S2-N1 (i.e., in the second set of bioinks) were produced to replicate the results obtained with the corresponding bioinks in the first set of bioinks. The absorbance measurements for the replicated experiments were taken at both 450 nm and 650 nm. Though the concentration of cell suspensions in the two sets of bioinks are different, there is a correlation in the behavior of the cells within the substrates of the two sets of bioinks in terms of increase or decrease in cell density. A clear observation suggests that the variation in cell concentration between day 1 and day 15 generally follow a similar pattern regardless of if a wavelength of 450 nm or 650 nm is

used to take absorbance readings. However, since *Chlorella* contains both chlorophyl a and chlorophyl b components, the disparity in the magnitude of the absorbance values for the same bioink at the different wavelengths of 450 nm or 650 nm can be attributed to a variation in the peak wavelength for the absorbance of the components of the chlorophyl types present in the *Chlorella* microalgae variant.

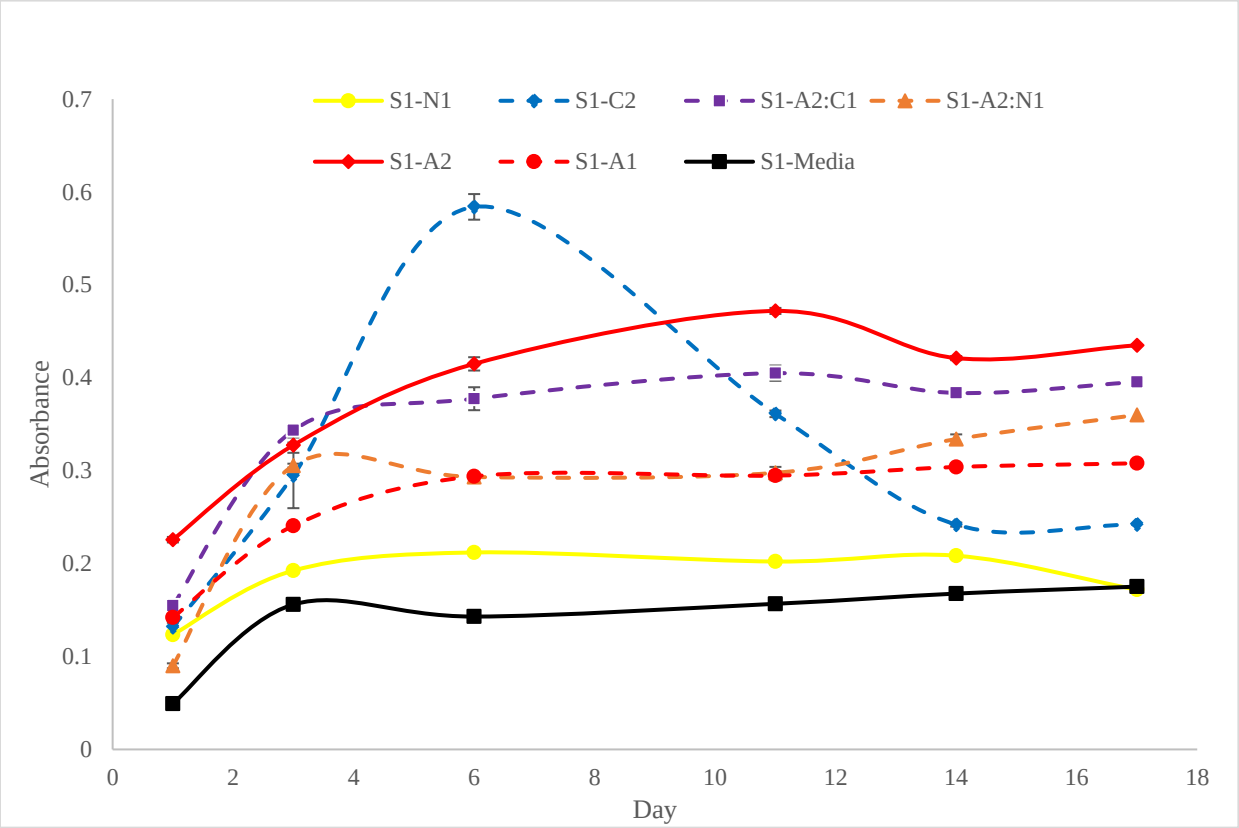

Figure 3.5. Relative variation of absorbance for the first set of bioinks at a wavelength of 450 nm and a cell count of $51.5 \times 10^6\ cells/mL$

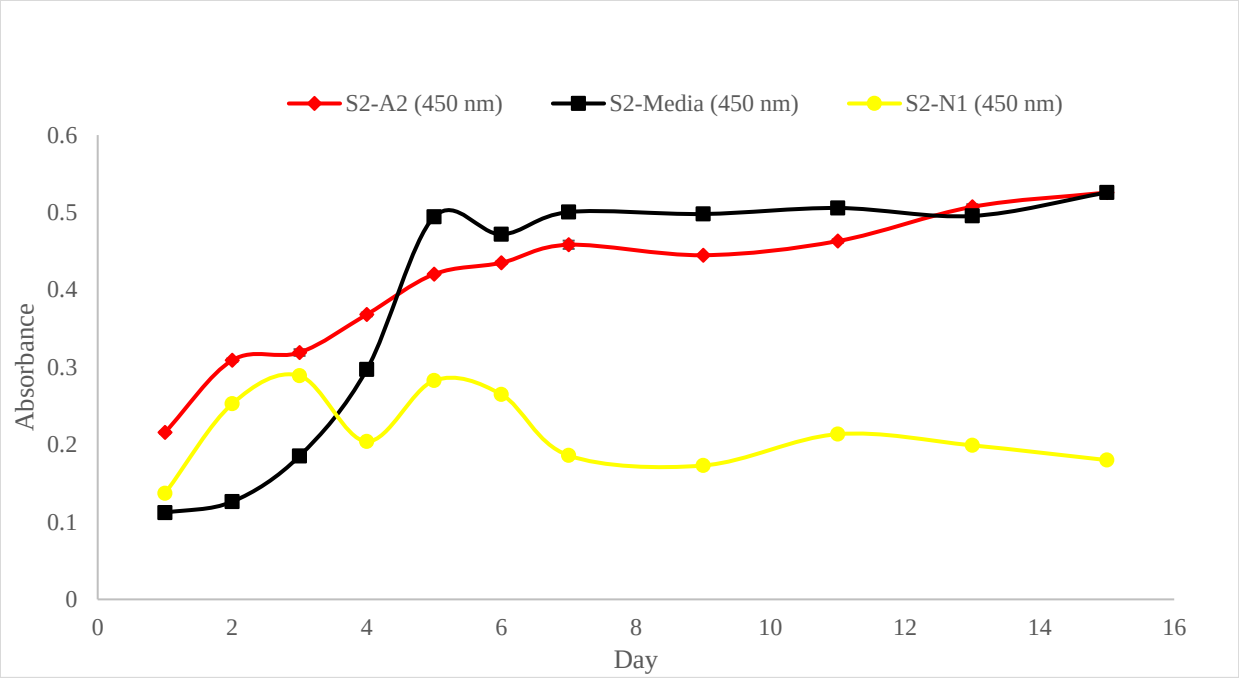

Figure 3.6. Replication of absorbance variation in 'Bioinks S1-A2, S1-Media and S1-N1' with 'Bioinks S2-A2, S2-Media, and S2-N1' respectively at a wavelength of 450 nm and a cell count of 55.3×10^6 $cells/mL$

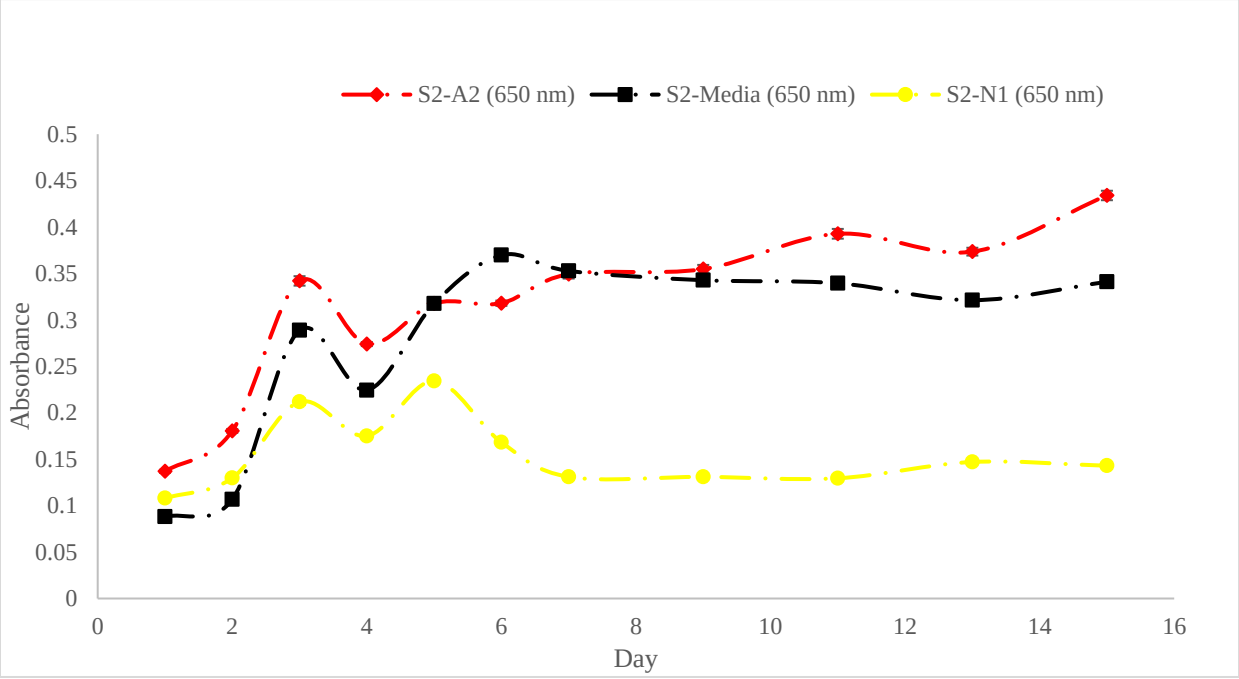

Figure 3.7. Replication of absorbance variation in 'Bioinks S1-A2, S1-Media and S1-N1' with 'Bioinks S2-A2, S2-Media, and S2-N1' respectively at a wavelength of 650 nm and a cell count of 55.3×10^6 $cells/mL$

In this section, Alginate's ability to support the rapid culture of *Chlorella* microalgae is emphasized and supported by absorbance-cell count calibration curves. Initially, Alginate demonstrates significant support for *Chlorella* microalgae culture, comparable to the culture Media alone. However, a noticeable trend emerges in that while Alginate initially promotes higher growth rates compared to Media, this trend diminishes after approximately day 6 (refer to Figure 3.5). Nevertheless, according to the trend observed in the curves, both Alginate and Media show a propensity to increase cell density until after day 14.

Conversely, NFC exhibits a hindering effect on *Chlorella* microalgae cell growth, as evidenced by a reduction in cell density in substrates with 1% NFC w/v shortly after day 3 (refer to Figure 3.5). However, Alginate and CMC substrates appear to generally support cell density increase. Interestingly, the substrate made with 2% CMC w/v exhibits a sharp increase in cell growth rate between day 1 and day 6, followed by a steep decrease thereafter.

Comparing the growth patterns of *Chlorella* cells in Media with substrates containing 2% Alginate/1% CMC w/v and 2% Alginate/1% NFC w/v, it appears that the presence of Alginate in a bioink substrate with NFC significantly mitigates NFC's inhibitory effect on algae cell growth.

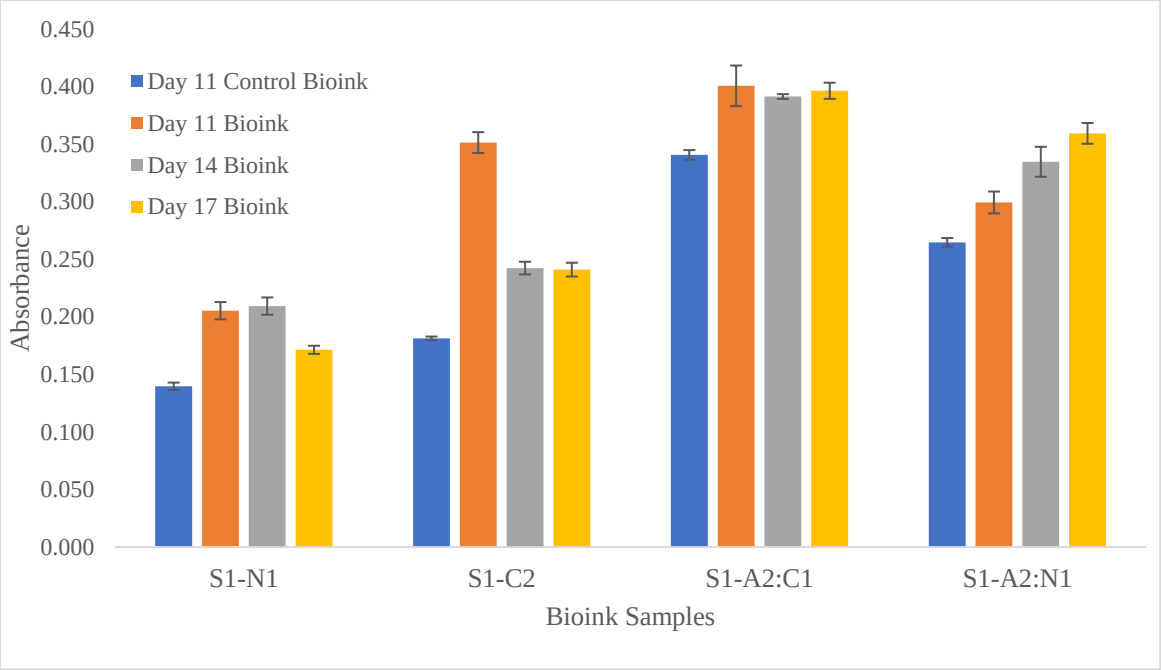

Figure 3.8. Discrete representation of cell density variation in significantly viscous set one bioinks (i.e. no subjection to nozzle tip printing pressure)

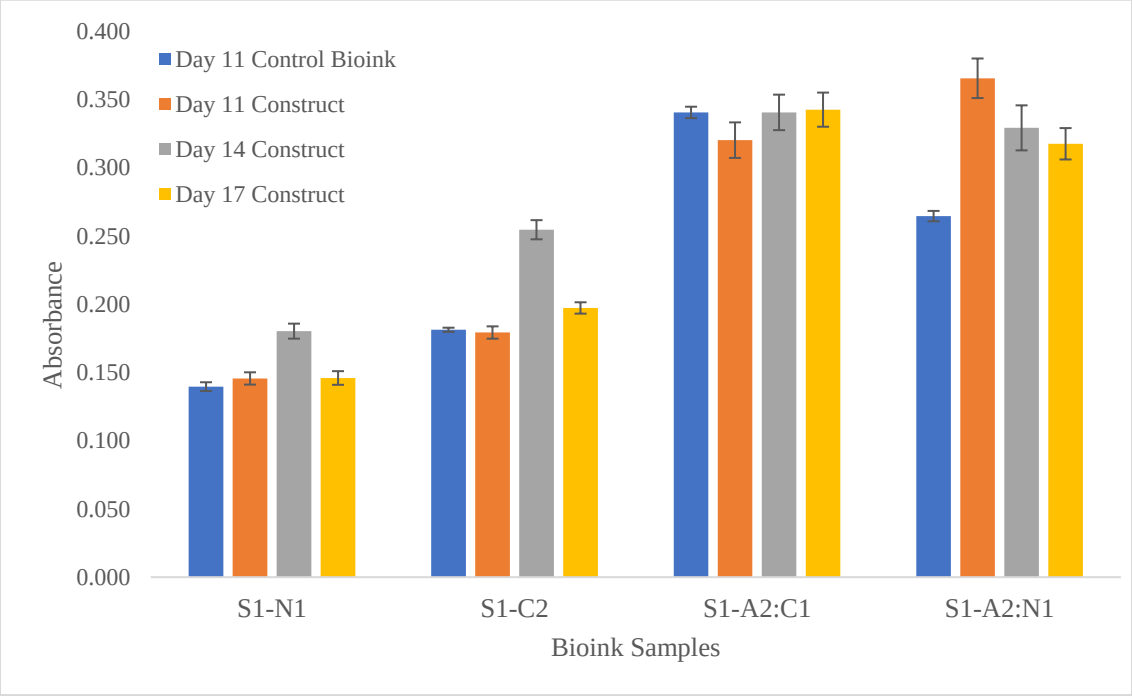

Figure 3.9. Discrete representation of cell density variation in constructs printed at 20 psi on day 11 of the cell culture from significantly viscous set one bioinks (i.e. after subjection to nozzle tip printing pressure)

On day 11 of the experiment, samples were taken from the bioinks S1-N1, S1-C2, S1-A2:C1, and S1-A2:N1. These samples were paired, and a portion was subjected to the printing process using a bioprinter to deposit the bioinks into cuvettes in a controlled manner, while the other portion was kept in a cuvette without printing. After printing at an extrusion pressure of 20 psi, the samples were returned to their respective culture conditions and allowed to continue incubating. Over the subsequent 6 days (from day 11 to day 17), cell density measurements were taken periodically with the aid on the spectrophotometer from both the printed and unprinted samples. The resulting data, represented in the bar charts of Figure 3.8 and Figure 3.9, illustrate the observed changes in cell density over this time frame, Bioinks S1-N1 and S1-C2 with substrate of 1% NFC and 2% CMC, respectively, show trend similar to each other for cell density variation after printing at 20 psi on day 11 of the culture – that is, an increase in cell concentration from day 11 to day 14 but a decline in cell concentration after day 14. In Bioink S1-A2:C1 with a substrate of 2% Alginate/1% CMC, there appears to be an onward increase in cell concentration after printing at 20 psi on day 11. Preprint and post-print bioink/construct samples have similar cell concentration variation trends in S1-N1, while the trend in Bioinks S1-C2 and S1-A2:C1 have no patterned order. However, there is a contrasting trend in cell density variation for Bioink S1-A2:N1 in the preprint bioink sample and the post-print construct. Alginate-only bioinks were excluded from this printability experiment because of their relatively low viscosity. Because patterned cell density variation trends could not be established from the samples subjected to bioprinting on the day 11 of culture, the next phase of experiments has been designed to include samples to be subjected to bioprinting on the day of the formulation of the bioink sample, so as to allow for an extended time to monitor cell density variation with printed constructs.

For an extensive understanding of the effect of the presence of NFC on cell density enhancement in bioink substrates, bioinks S2-N1:C0.5, S2-N1:C0.25 and S2-N1:A3 were developed using substrates respectively derived from 1% NFC/0.5% CMC w/v, 1% NFC/0.25% CMC w/v and 1% NFC/3% Alginate w/v. Figure 3.10 compares the growth curve of the bioinks with measurement wavelengths of 450 nm and 650 nm. Results indicate that NFC tries to reverse cell multiplication in all three samples of bioinks, but the presence of 3% Alginate w/v in bioink S2-N1:A3 appears to have forced a comeback for an onward increase in cell density around day 12. The cell growth pattern with a combination of 0.25% CMC w/v with 1% NFC w/v in Bioink S2-N1:C0.25 appears to be more desirable than in a combination of 0.5% CMC w/v with 1% NFC w/v in Bioink S2-N1:C0.5 because the former causes a larger increase in cell density between day 1 and day 14 than the later.

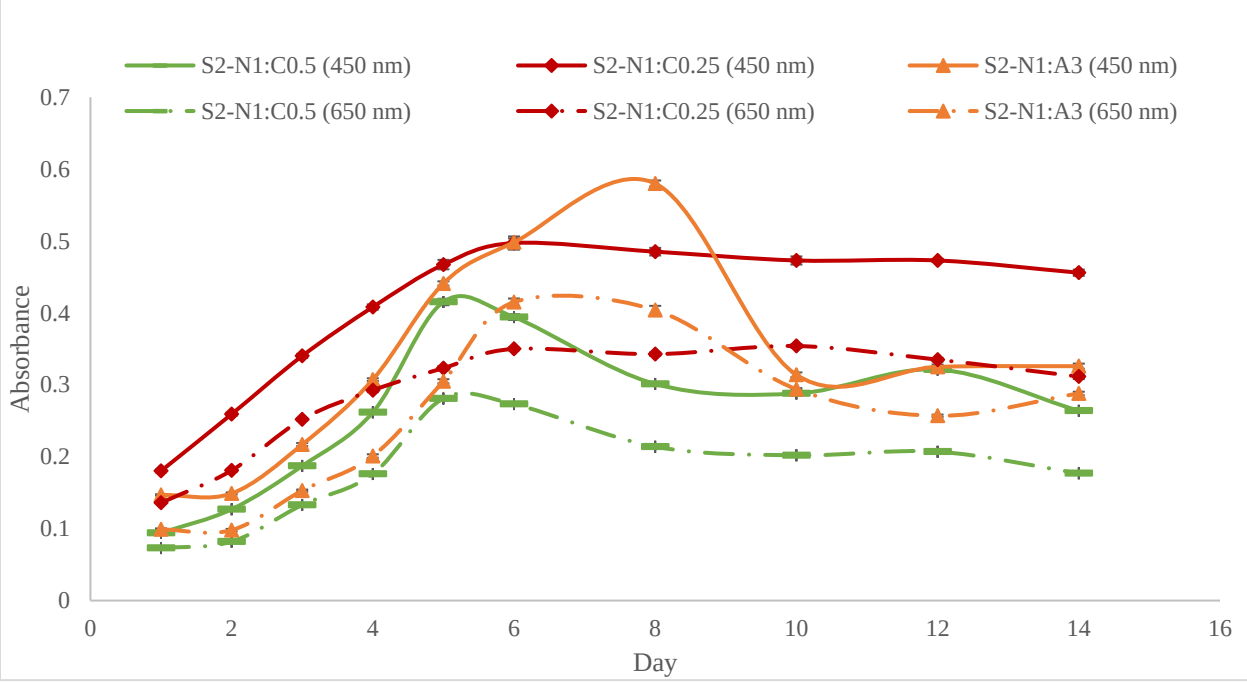

Figure 3.10. Representation of the effect of NFC content in bioink substrates on cell density variation

Earlier attempts were made to understand the growth pattern of cell suspensions in constructs printed with Bioinks S1-N1, S1-C2, S1-A2:C1 and S1-A2:N1, but the bioprinting of the constructs took place on Day 11 of the culture process. To understand the cell growth pattern in bioinks printed into constructs immediately after addition of cell suspensions to the substrates, Bioinks S2-A3:C0.5:N0.5 and S2-A3:C0.25:N0.5 with substrates respectively derived from 3% Alginate/0.5% CMC/0.5% NFC and 3% Alginate/0.25% CMC/0.5% NFC were bio-printed at different printing pressure. The bioink samples were deposited into cuvettes at 20 psi in a first batch, and shortly after into a separate set of cuvettes, at 30 psi in a second batch. Results obtained from the monitoring of the cell growth pattern of the printed constructs, given in Figure 3.10 suggest that with the proportion of Alginate and NFC kept constant at 3% w/v and 0.5% w/v, respectively, a lower proportion of CMC (i.e. 0.25% w/v) enhances cell density better than a higher proportion (i.e. 0.5% w/v of CMC), possibly because the nozzle tip pressure causes a refinement of the crystalline structure of the NFC components of the bioinks to allow for a better enhancement of proliferation of cells within the bio-printed construct. However, a lower CMC to NFC ratio generally appears to enhance cell density.

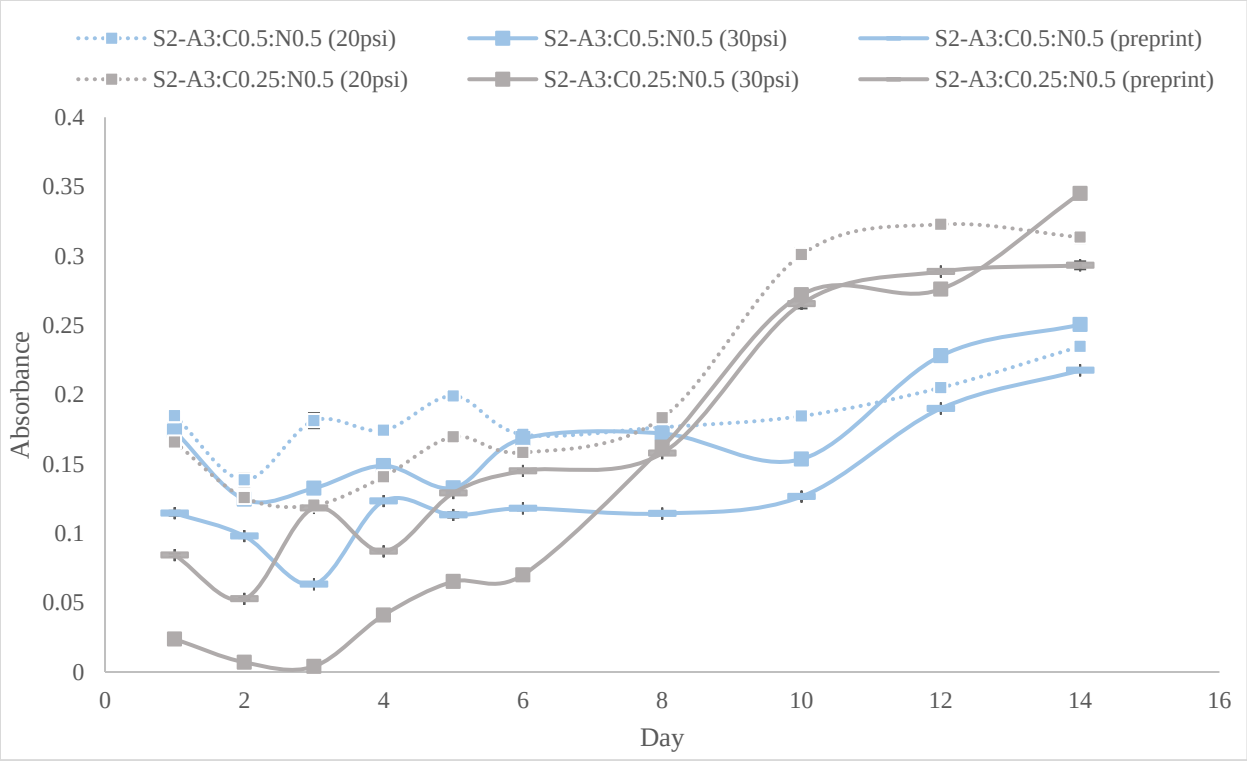

Figure 3.11. Cell density variation in microalgae constructs derived from tri-hydrogel substrate, bio-printed at different printing pressures

Figures 3.12 and 3.13 depict calibration curves illustrating the quantitative relationship between absorbance readings and cell counts of *Chlorella* microalgae-based bioinks. To provide clarity on data generation, it's important to note that the methods section outlines the steps followed in producing these results. Specifically, absorbance measurements were obtained using a spectrophotometer, while cell counts were determined through direct counting using a hemocytometer.

To enable more direct estimates of cell count in Alginate 1% w/v, Alginate 2% w/v, and Media using absorbance data from the spectrophotometer, several steps were followed to obtain calibration curves relating absorbance to cell count. These steps include preparing bioinks from solutions based on Alginate 1% w/v, Alginate 2% w/v, and Media, and then measuring absorbance with the spectrophotometer. Estimate of cell count had been previously recorded

through direct counting using a hemocytometer. Dilution of the suspension was done when needed to ensure absorbance falls within the data range intended to be captured with the curves. Bioink samples derived from Alginate and Media have been used for these calibrations because, due to their low viscosity, they make it relatively easy to carry out manual cell count using hemocytometry.

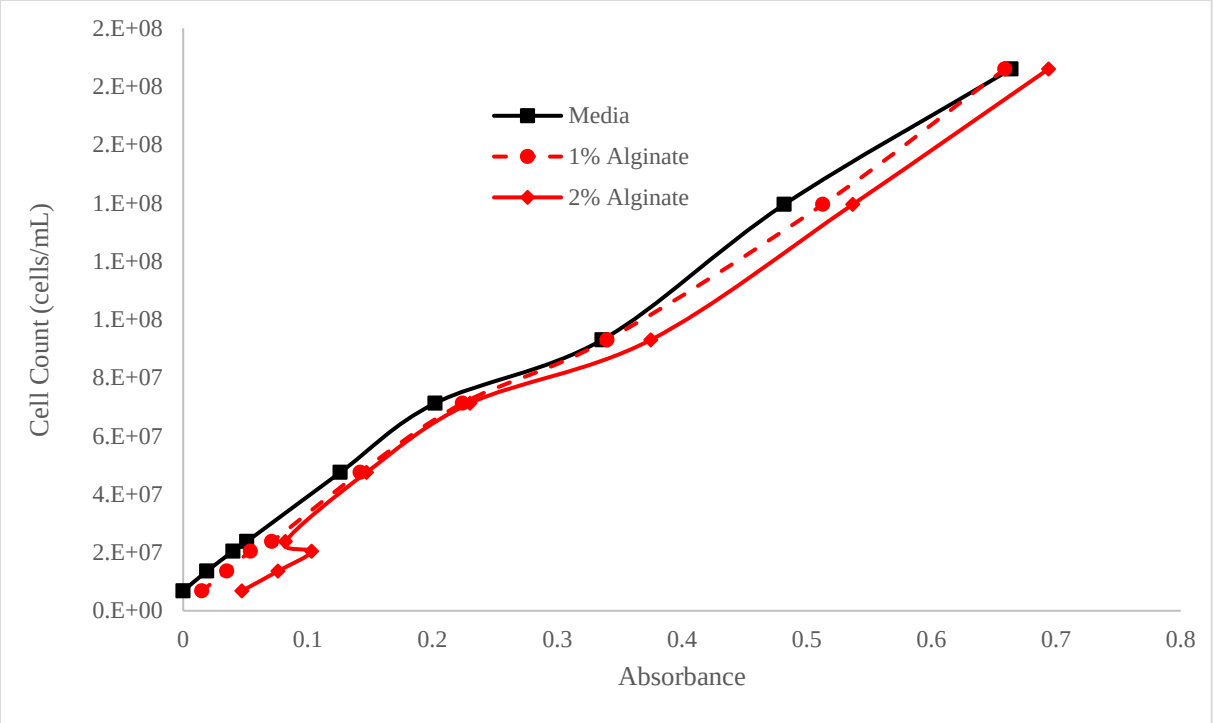

Figure 3.12. Cell Count-Absorbance calibration curve (absorbance recorded at a wavelength of 450 nm)

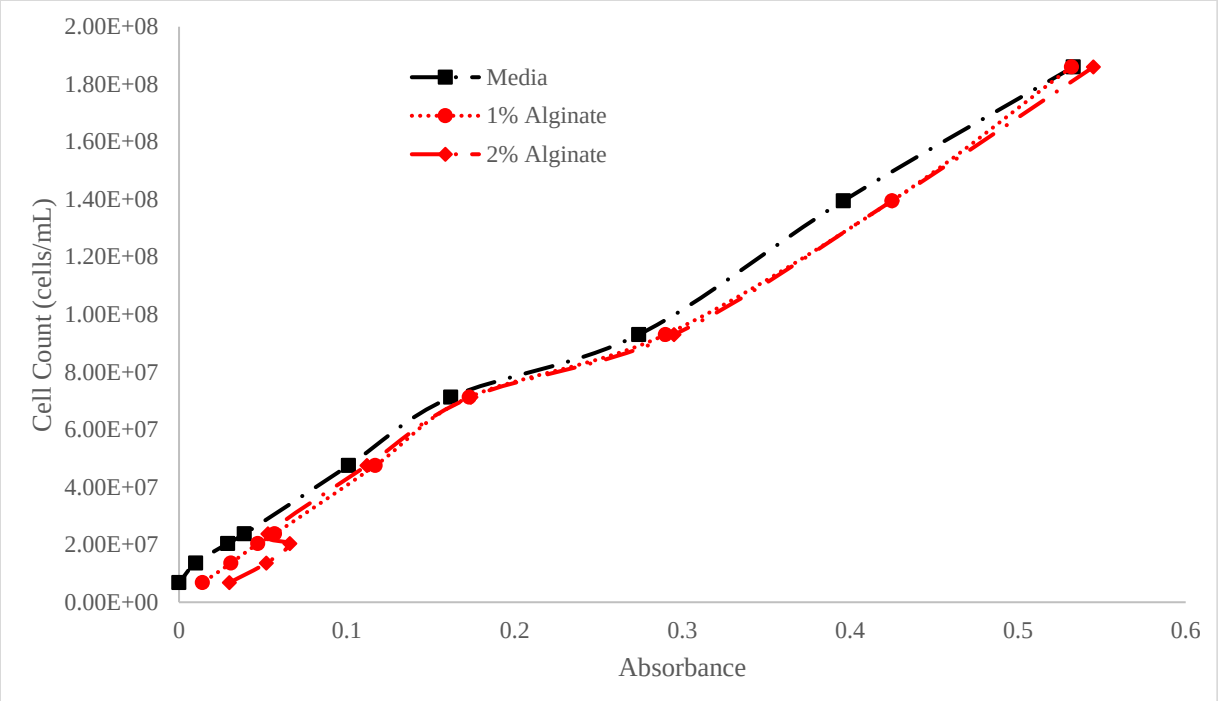

Figure 3.13. Cell Count-Absorbance calibration curve (absorbance recorded at a wavelength of 650 nm)

The calibration curves reveal a consistent relationship between absorbance and cell count across the selected bioinks, including those with substrates derived from Media, Alginate 1% w/v, and Alginate 2% w/v. This consistency suggests that variations in cell count correspond closely with changes in absorbance levels across all substrates. The parallel rates of variation observed underscore the reliability of absorbance as a proxy for cell count estimation, regardless of the substrate composition. These findings affirm the utility of spectrophotometric analysis for quantifying microalgae concentration in bioinks, offering a standardized approach applicable across different substrate formulations. Such insights enhance the robustness and versatility of cell count estimation methods in bioink development.

3.3. Printability Study

Numerous bioprinting trials were conducted to comprehensively assess the suitability of selected experimental bioinks. A systematic analysis in this study incorporated evaluation of rheological, geometrical, and physical properties to gauge printability. This multifaceted approach allowed for a thorough understanding of how the biomaterials perform within the printing process, aiding in the selection of bioinks optimized for the study's objectives.

3.3.1. Rheological Characteristics of Experimental Bioinks

Figures 3.14 and 3.15. Interestingly, the microalgae suspension exhibits notably higher shear stress values and viscosity compared to both the hydrogel substrates and the corresponding experimental bioinks. Despite the initially higher viscosity of the cell suspension, the viscosity of the resulting bioink decreased upon seeding microalgae cells into the substrates. This suggests that the addition of cells to the hydrogel substrates alters the viscosity of the resultant bioink, potentially due to interactions between cells and polymer chains or the introduction of water into the system. This phenomenon, termed shear thinning or pseudoplastic behavior, has been observed in other studies involving hydrogel-cell interactions and bioprinting methodologies [98]. Importantly, it highlights that the printability achieved with the hydrogel substrate before cell addition may not translate to cell-laden bioink made from the same hydrogel substrate. Therefore, the addition of a very high viscosity cell suspension to the substrates does not guarantee improved printability or enhanced shape fidelity.

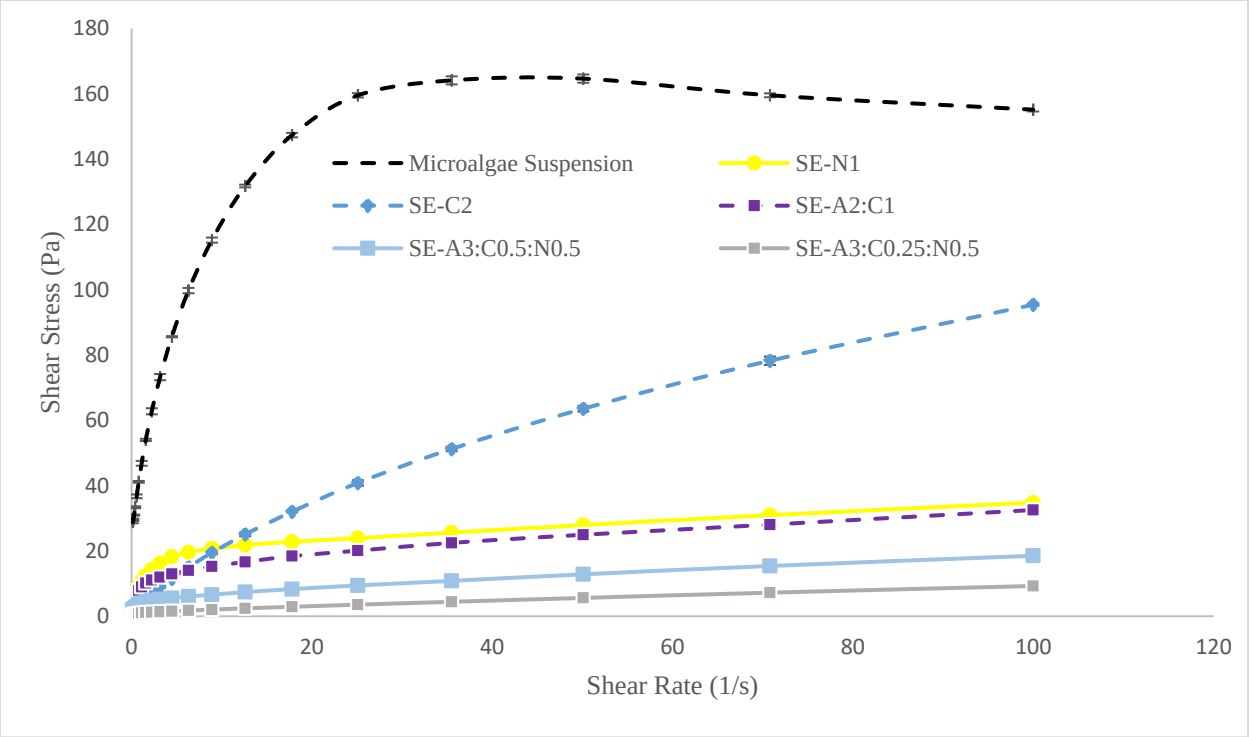

Figure 3.14. Comparison of rheological characteristics of bioinks used for experimental bioprinting

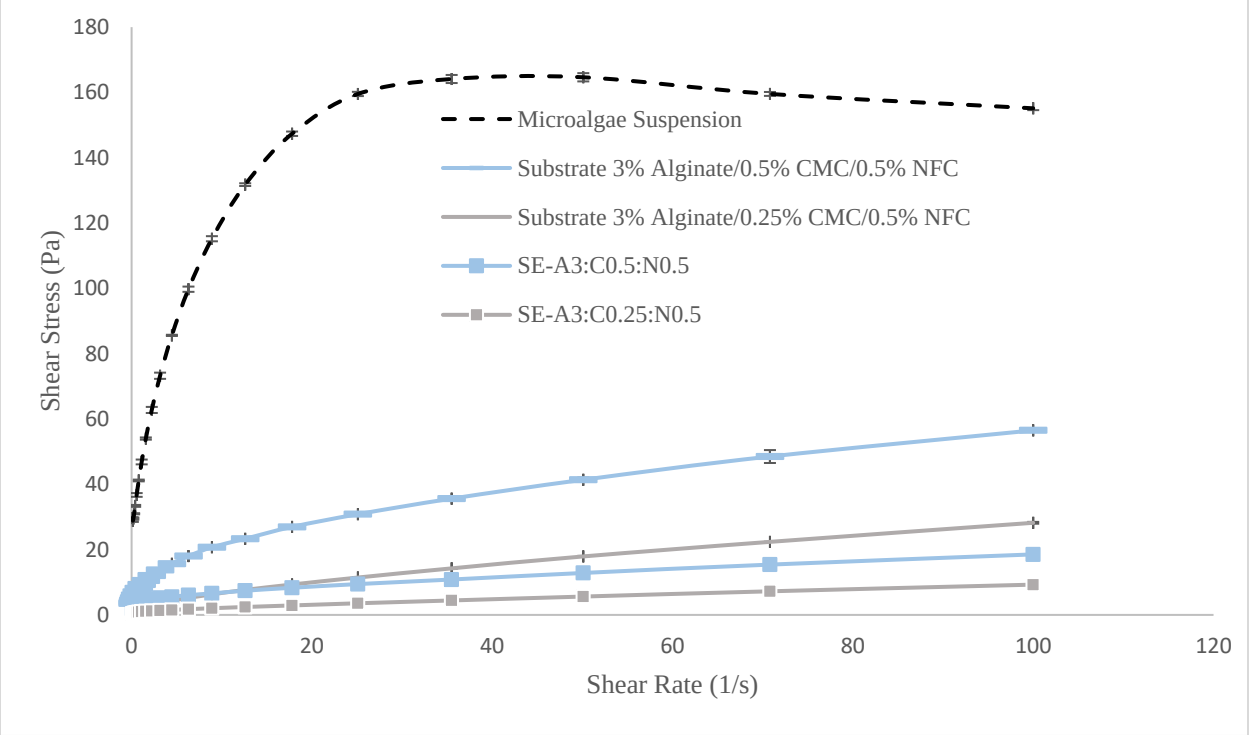

Figure 3.15. Comparison of rheological characteristics of experimental Bioinks and respective tri-hydrogel substrate

3.3.2 Experimental Bioprinting with *Chlorella*-based Bioinks

In this study, bioprinting trials were conducted using five experimental bioinks, specifically formulated for the purpose of 3D bioprinting. Notably, these bioinks were distinct from the previously discussed formulations containing specific cell counts:

- Bioink SE-N1 (from 1% NFC)
- Bioink SE-C2 (from 2% CMC)
- Bioink SE-A2:C1 (from 2% Alginate and 1% CMC)
- Bioink SE-A3:C0.5:N0.5 (from 3% Alginate, 0.5% CMC and 0.5% NFC)
- Bioink SE-A3:C0.25:N0.5 (from 3% Alginate, 0.25% CMC and 0.5% NFC)

Interestingly, none of these specially formulated bioinks, derived from bi-hydrogel or tri-hydrogel substrates, exhibited desirable printability characteristics. This may be attributed to the significant reduction in viscosity induced by the Alginate components of the substrates. Similarly, NFC, although ineffective for algae cell growth, also failed to sufficiently influence shape fidelity as a standalone substrate at the optimal 1% w/v composition. Among the experimental bioinks, the 2% CMC w/v formulation produced the fairest constructs, albeit compromised by environmental factors affecting cohesion.

Figure 3.16 illustrates a 3D model of a bio-printed construct with 90% porosity. Figures 3.17 and 3.18 depict comparative bioprinting of 'non-Alginate' bioinks at 15 psi, while Table 3.2 details physical properties, aiding assessment of printability and performance. This systematic bioink evaluation sets a foundation for advanced bioprinting technologies.

Printability is important in determining the success of fabricating intricate tissue constructs with desired characteristics. The results provided in this study provide insights into the factors

influencing printability and highlight the experimentation and analysis involved in assessing bioprinting outcomes with respect to the experimental bioinks adopted for this study.

The physical properties of bioinks, detailed in Table 3.2, serve as fundamental parameters influencing printability. These properties include extrusion pressure, mass measurements, volume measurements, density of bioink, and percentage difference in construct volume. Variations in bioink composition and formulation appear to directly impact these properties, and this influences the rheological behavior and structural characteristics of the bioinks. By taking note of these properties across different formulations, comprehensive understanding can be gained as to how bioink properties affect printability outcomes.

Extrusion pressure emerges as a critical parameter affecting flow rate, deposition accuracy, and structural fidelity in bioprinting. Standardizing extrusion pressure at 15 psi across the various bioink formulations allows for the isolation of the effects of other factors on printability. This approach facilitates comparative analysis, enabling a discernment of subtle differences in printability that could be attributed to variations in bioink composition and formulation. By controlling extrusion pressure, a systematic evaluation of how bioink properties influence extrusion behavior and printability outcomes is made possible.

The mass and volume measurements provided in Table 3.2 offer tangible evidence of differences in composition, formulation, and printability across bioink formulations. Discrepancies between actual and theoretical construct volumes highlight the accuracy of the printing process and provide insights into the deviation from intended designs. These measurements serve as quantitative indicators of printability, enabling an assessment of the efficacy of bioink formulations in realizing desired construct geometries and dimensions.

Real-time observations of adhesive characteristic changes during bioprinting, depicted in Figure 3.19, offer qualitative insights into the dynamic nature of printability. Changes in adhesive characteristics directly impact extrusion behavior, structural integrity, and overall printability. By understanding these dynamic phenomena, the refinement of bioink formulations can be guided and printing parameters can be regulated to optimize printability outcomes.

Comparative bioprinting analyses presented in Figures 3.17 and 3.18 further elucidate printability outcomes by comparing the performance of 'non-alginate' bioinks at a standardized extrusion pressure of 15 psi. These figures provide insights into extrusion smoothness, structural integrity, and overall printability of different bioink formulations. Identifying trends, patterns, and outliers in printability outcomes allows researchers to pinpoint optimal formulations and process parameters conducive to achieving desired printing outcomes.

This systematic approach for the evaluation of printability outcomes in bioprinting with incidentally low viscosity experimental bioinks enhances a fundamental understanding of the factors influencing the potential fabrication of tissue constructs with green plant cells. Leveraging this knowledge, researchers in tissue bioprinting can be informed about the optimization of bioink formulations, as well as printing parameters with the aid of custom 3D bioprinters.

Table 3.2. Physical properties of experimental bioinks and process variables for experimental bioprinting

	Boink SE-N1	Boink SE-C2	Bioink SE-A2:C1	Bioink SE-A3:C0.5:N0.5	Bioink SE-A3:C0.25:N0.5
Extrusion pressure (psi)	15	15	15	15	15
Mass of empty tube (g)	6.491	6.544	6.535	6.53	6.46
Mass of loaded bioink tube (g)	17.275	17.841	17.381	17.556	17.004
Net mass of bioink in tube (g)	10.784	11.297	10.846	11.026	10.544
Volume of bioink in tube (mL)	11	11.5	11	11	10.5
Density of bioink (g/mL)	0.980364	0.982348	0.986	1.002364	1.00419
Mass of empty petri dish (g)	8.091	8.013	8.016	8.076	7.894
Mass of petri dish with construct (g)	9.559	8.213	11.567	12.06	11.593
Net mass of construct (g)	1.468	0.2	3.551	3.984	3.699
Actual volume of construct (mL)	1.497404	0.203594	3.60142	3.974605	3.683564
Theoretical volume of construct (mL)	0.08	0.08	0.08	0.08	0.08
Percentage difference in volume of construct (%)	1871.754	254.4923	4501.775	4968.257	4604.455

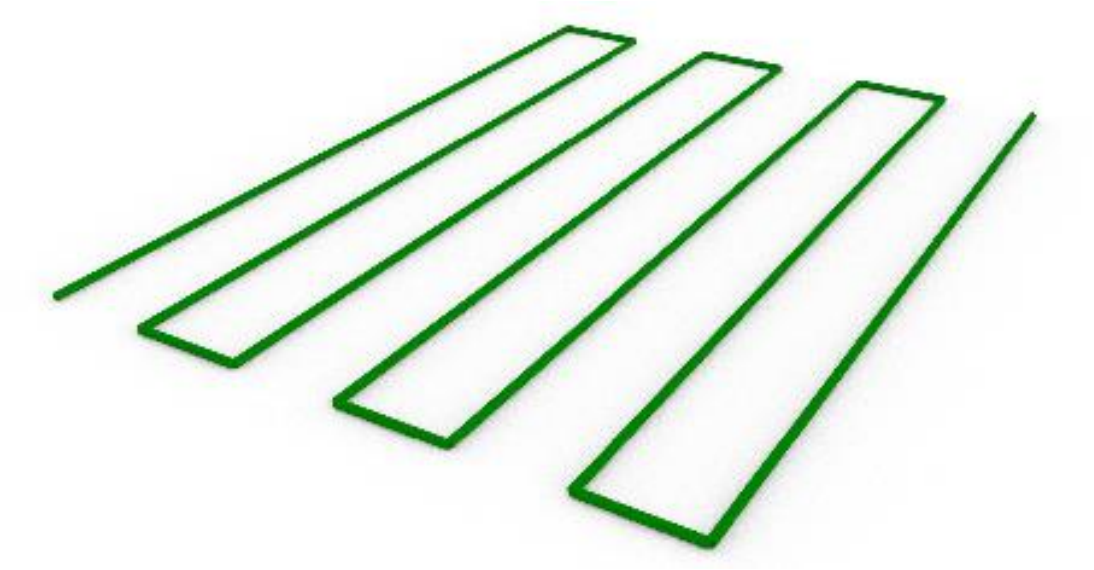

Figure 3.16. 3D model for experimental bioprinting construct

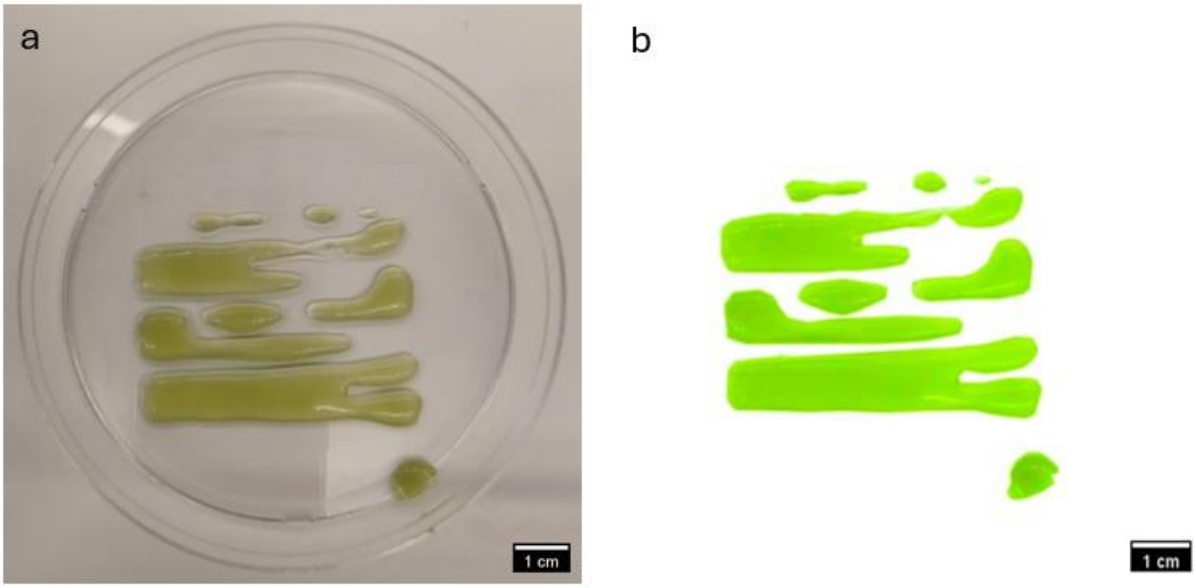

Figure 3.17 (a & b). Image of experimental construct from Bioink SE-N1 (bioprinted from experimental bioink derived from 1% NFC w/v)

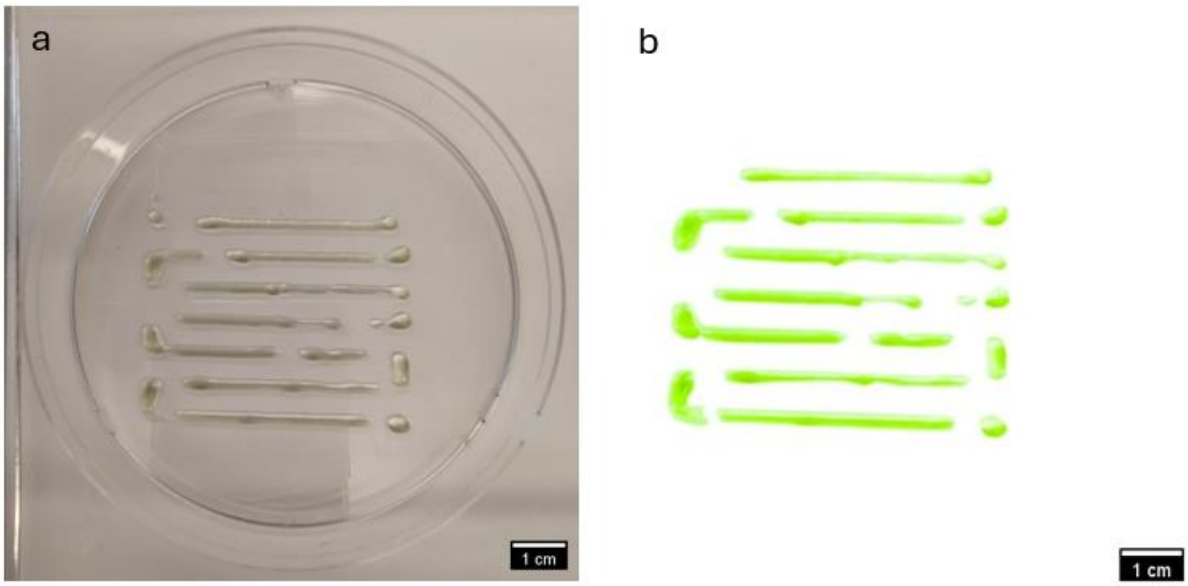

Figure 3.18 (a & b). Image of experimental construct from Bioink SE-C2 (bioprinted from experimental bioink derived from 2% CMC w/v)

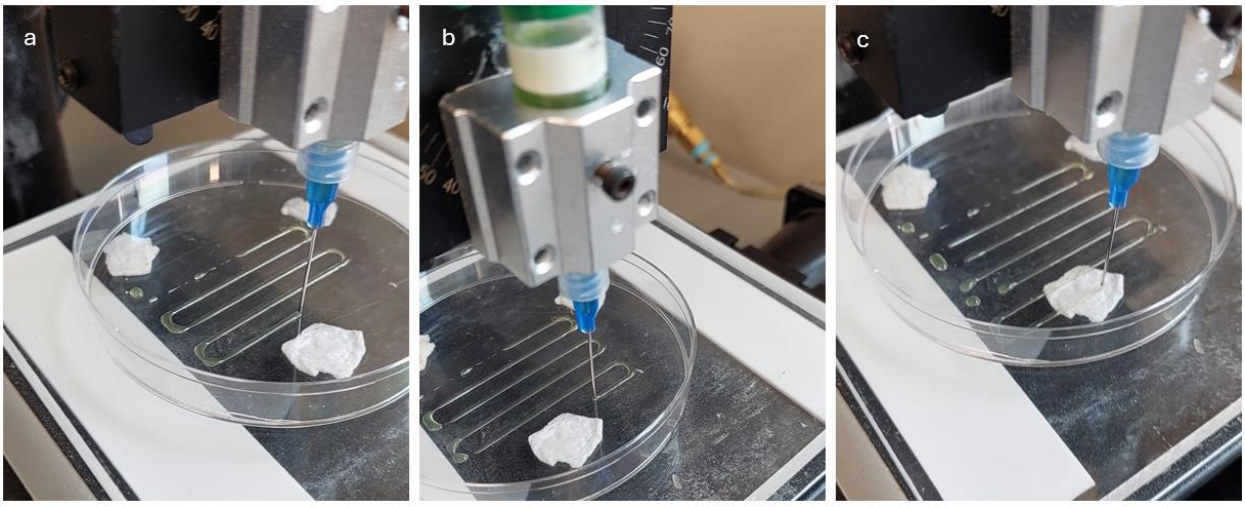

Figure 3.19. Stages during experimental bioprinting of *Chlorella*-based bioink, derived from 2% CMC w/v, showing points before construct loses cohesion (a), starts to lose cohesion (b), and has significantly lost cohesion (c)

CHAPTER 4

DISCUSSION

4.1. Growth Pattern of *Chlorella* Cells in Hybrid Scaffolds

The exploration of *Chlorella* microalgae growth within hybrid hydrogel scaffolds is integral to advancing bioprinting techniques for tissue engineering and regenerative medicine applications. This study delved deeply into the intricate dynamics of Alginate, CMC, and NFC in influencing cell survival and proliferation within bioinks and printed constructs. By meticulously tracking periodic absorbance variations and correlating them with cell concentration changes, invaluable insights was gained into the underlying mechanisms shaping *Chlorella* cell growth dynamics within the scaffolds.

Alginate, known for its biocompatibility and ability to provide a supportive matrix for cell growth, emerged as a frontrunner in the study. The presence of Alginate in the hydrogel formulations significantly enhanced *Chlorella* cell proliferation, attributed to its capacity for nutrient retention and stimulation of metabolic activity. This finding underscores the importance of selecting hydrogel components that offer an optimal microenvironment for cell viability and proliferation in bioprinted constructs. Previous studies [99], as summarized in Table 4.1, corroborate the suitability of Alginate for the post-fabrication culture of cells of different plant species.

Conversely, the introduction of NFC introduced intriguing complexities to the growth dynamics. While NFC is known for its structural reinforcement properties, observations revealed a reduction in cell density within NFC-containing bioinks. This unexpected outcome underscores the need for a nuanced understanding of the interactions between hydrogel components and cell

behavior, highlighting the challenges associated with optimizing hybrid hydrogel formulations for bioprinting applications.

Furthermore, the utilization of CMC in bioink formulations resulted in distinct growth trajectories characterized by fluctuating cell concentrations over time. This variability underscores the dynamic nature of cell-hydrogel interactions and emphasizes the importance of fine-tuning bioink compositions to achieve desired growth outcomes. By elucidating the complex interplay between hydrogel components and *Chlorella* cell growth, this study provides valuable insights that can inform the development of more effective bioink formulations for bioprinting applications.

Table 4.1. Evidence of the suitability of Alginate for post-biofabrication culture

Field of Application	Plant cell type	Plant species	Hydrogel substrate	Reference
Agri-food manufacturing	Land Plant	*Daucus carota L (Carrots)*	Sodium Alginate 4% w/v	[100]
Textile/Biodesign	Microalgae	*Chlamydomonas reinhardtii*	Sodium Alginate 2.5% w/v	[101]
Morphological studies	Land Plant	*Ocimum basilicum (Basil)*	Sodium Alginate 28% w/w, Agarose 0.9% w/w, and Methylcellulose 3% w/w	[102]
Biomanufacturing	Microalgae	*Chlamydomonas reinhardtii and Chlorella sorokiniana*	Sodium Alginate 3% w/v, and Methylcellulose 9% w/v	[103, 104]

4.2. Effects of Extrusion Pressure on Post-printing Cell Multiplication

Examining the influence of extrusion pressure on post-printing cell multiplication sheds light on the intricate dynamics of the bioprinting process. Alginate's low viscosity facilitated uniform cell distribution within printed constructs, with micro-extrusion pressures playing a pivotal role in

enhancing cell multiplication rates. Findings in this study suggest that higher extrusion pressures result in more favorable outcomes, with increased cell proliferation observed over time.

Surprisingly, bioinks containing CMC or NFC showcased resilience to varying extrusion pressures, with sustained cell proliferation observed across different pressure settings. This resilience underscores the robustness of these hydrogel formulations and highlights their potential for supporting cell growth in bioprinted constructs under varying printing conditions. Anja Lode et. al. [103] had investigated the growth rate of *Chlamydomonas reinhardtii and Chlorella sorokiniana*, from a micro-extrusion 3D bioprinting context, and found that the viability of embedded algae was comparable (and sometimes higher) to that of algae in suspended culture. The 3D-printed construct of *Chlamydomonas reinhardtii* from their study is shown in Figure 4.1, with hydrogel substrate made from Sodium Alginate (3% w/v) and Methylcellulose (9% w/v).

These findings have significant implications for optimizing bioprinting processes, as they provide valuable insights into the interplay between extrusion pressure, hydrogel properties, and cell behavior. By elucidating the complex dynamics at play during the bioprinting process, this study contributes to paving the way for the development of more effective strategies for fabricating tissue-engineered constructs with enhanced biological functionality.

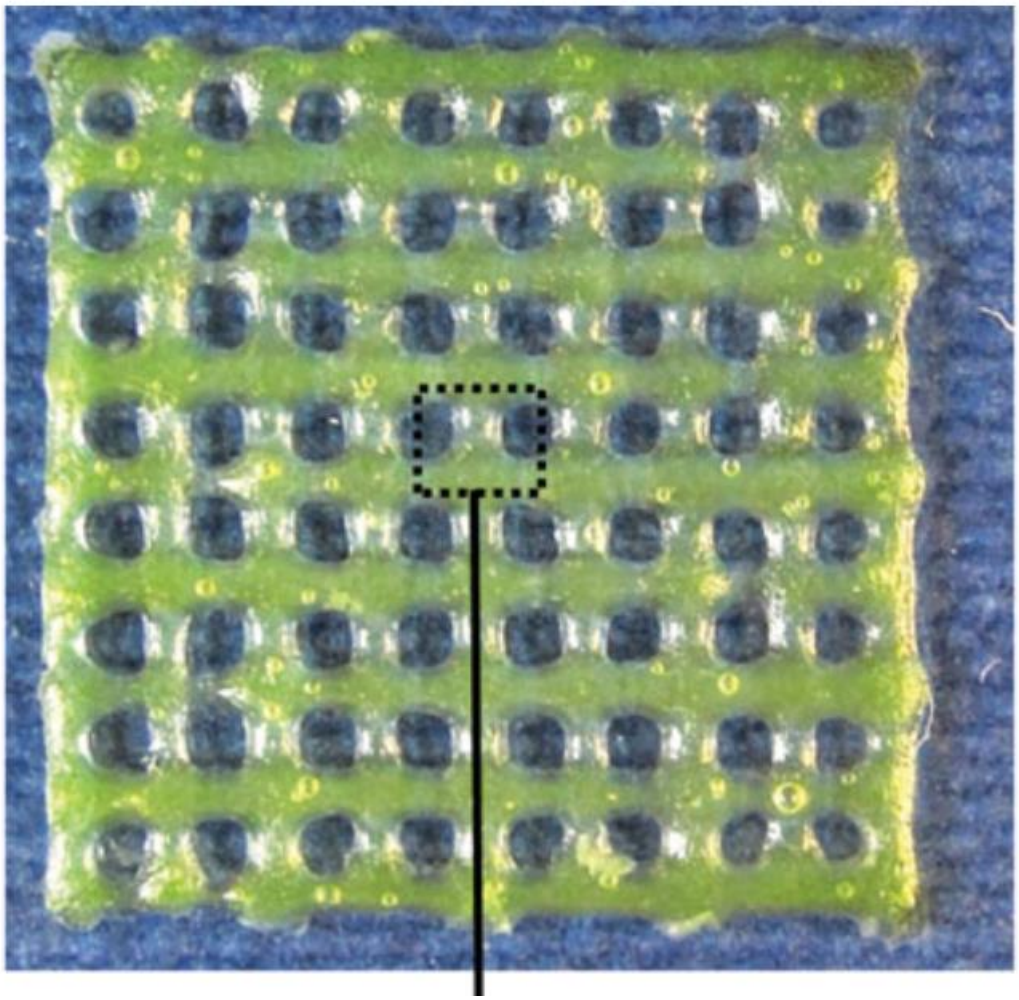

Figure 4.1. 3D-printed construct of *Chlamydomonas reinhardtii* with scaffolding made from Sodium Alginate (3% w/v) and Methylcellulose (9% w/v) [103]

CHAPTER 5

CONCLUSIONS

In this comprehensive investigation, the intricate dynamics governing the utilization of hybrid hydrogel scaffolds in the realm of *Chlorella* microalgae cell proliferation was delved into, particularly under the mechanical stresses intrinsic to 3D bioprinting. The meticulous selection of three hydrogel biomaterials—Alginic acid sodium salt (ALGINATE), Nanofibrillated Cellulose (NFC) – TEMPO, and CarboxyMethyl Cellulose (CMC)—was underpinned by their well-documented scaffolding capabilities, aiming to decipher their individual and synergistic impacts on cell density and morphology.

The experimental design encompassed the formulation of two sets of bioinks, each carefully tailored to scrutinize the effects of distinct hydrogel compositions on cell behavior. The first set, comprising six hydrogel-based bioinks supplemented with a *Chlorella* cell suspension in Alga-Gro freshwater medium, served as our primary investigative platform. In parallel, the second set was conceived to validate and extend the insights gleaned from the initial experimentation phase.

Integral to analyses carried out was the strategic acquisition and interpretation of absorbance data obtained from spectrophotometer readings, serving as a quantitative metric for elucidating the growth patterns of algae cells within diverse hydrogel compositions. Calibration curves for three of the bioink formulations facilitated an analogical understanding of the nuanced relationship between absorbance values and cell count, offering invaluable insights into cell proliferation dynamics. Concurrently, rheometer tests provided a deeper understanding of the shear thinning properties inherent to our hydrogel compositions, enriching our comprehension of their rheological behavior under different stress conditions.

Findings underscored the pivotal role of Alginate as a potent substrate in fostering accelerated cell density and concentration, primarily attributable to its facilitation of cell proliferation and morphology enhancement. However, the inherent low viscosity of Alginate-only bioinks rendered them unsuitable for 3D bioprinting applications, underscoring the necessity of judicious hydrogel selection in bioink formulation. Notably, CMC exhibited an intriguing pattern of an initial surge in cell density followed by a subsequent decline, shedding light on the nuanced interplay between hydrogel compositions and cell behavior. Nevertheless, hybrid substrates combining Alginate and CMC demonstrated superior performance, surpassing the limitations inherent to CMC-only bioinks.

The investigation into NFC yielded promising insights into its role in maintaining cell proliferation, albeit with caution regarding its proportion in a mixture. Excessive proportions of NFC within hybrid substrates were found to impede cell growth, underscoring the delicate balance required in bioink formulation. The adhesive properties inherent to NFC and CMC emerged as critical determinants of cell distribution within bioinks, emphasizing the importance of substrate composition in dictating cell behavior.

Looking ahead, this study advocates for further exploration aimed at providing a framework for the optimal proportion of CMC within hybrid substrates for microalgae-based bioinks. Moreover, a need is seen for a paradigm shift towards prioritizing printability over cell growth enhancement in bioink optimization endeavors, emphasizing the need to precisely calibrate rheological properties while maximizing cell proliferation and differentiation potential.

By unraveling the intricate interplay between hydrogel compositions and cell behavior, this study considerably contributes to charting the way forward for refined bioprinting techniques, poised to revolutionize tissue engineering and regenerative medicine landscapes.

REFERENCES

1. S. Mandal, G. K. Nagi, A. A. Corcoran, R. Agrawal, M. Dubey, and R. W. Hunt, "Algal polysaccharides for 3D printing: A review," *Carbohydr. Polym.*, vol. 300, pp. 120267, Jan. 15, 2023, doi: 10.1016/j.carbpol.2022.120267.

2. M. Hannon, J. Gimpel, M. Tran, B. Rasala and S. Mayfield, "Biofuels from algae: challenges and potential," *Biofuels*, vol. 1, no. 5, pp. 763-784, 2010.

3. S. Chen, C. Liu, J. Pan, Y. Chen, J. Wang, H. Wang, and F. Xing, "A review on 3D bioprinting of functional skin tissue," Advanced Healthcare Materials, vol. 9, no. 19, pp. 2000802, 2020.

4. Y. S. Zhang, K. Yue, J. Aleman, K. Mollazadeh-Moghaddam, S. M. Bakht, J. Yang, W. Jia, V. Dell'Erba, P. Assawes, S. R. Shin, M. R. Dokmeci, R. Oklu, and A. Khademhosseini, "3D bioprinting for tissue and organ fabrication," Annals of Biomedical Engineering, vol. 45, no. 1, pp. 148-163, 2019.

5. F. J. R. Choix, M. G. García, J. C. García, and J. C. García, "Bioprinting: A new approach to bone tissue engineering," Cytotherapy, vol. 20, no. 1, pp. S140-S141, 2018.

6. D. H. Kim and Y. R. Kim, "Development of an eco-friendly biosensor for monitoring environmental pollution," Journal of Hazardous Materials, vol. 332, pp. 125-130, 2017.

7. V. Lindsey, "Will your future clothes be made of algae?" *University of Rochester*, April 29, 2021. https://www.rochester.edu/newscenter/will-your-future-clothes-be-made-of-algae-476562/

8. T. Bito, E. Okumura, M. Fujishima and F. Watanabe, "Potential of *Chlorella* as a dietary supplement to promote human health," *Nutrients*, vol. 12, no. 9, p. 2524, 2020.

9. M. I. Alkhalf and F. K. Khalifa, "Blueberry extract attenuates γ-radiation-induced hepatocyte damage by modulating oxidative stress and suppressing NF-κB in male rats, "*Saudi journal of biological sciences*, vol. 25, no. 7, pp.1272-1277, 2018.

10. S. Michelle, *Chlorella* found to dramatically improve cardiovascular health", October 28, 2017. *Chlorella* found to dramatically improve cardiovascular health – NaturalNews.com

11. J. Groll, T. Boland, T. Blunk, J. A. Burdick, D. W. Cho, P. D. Dalton, B. Derby, *et al*. "Biofabrication: reappraising the definition of an evolving field." *Biofabrication* vol. 8, no. 1, pp. 013001, 2016;

12. J. M. Lee, S. L. Sing, M. Zhou and W. Y. Yeong, "3D bioprinting processes: A

perspective on classification and terminology," *International journal of imprinting*, vol. 4, no. 2, 2018.

13. S. William, A. Aarley, L. B. Chi Chung, J. B. Toombs, D. Cathal, C. O'Connell, K. Hayden K. B. Taylor, E. Daniel, A. Heath, J. David, A. Collins, "Advances in biofabrication techniques towards functional bioprinted heterogeneous engineered tissues: A comprehensive review", *Bioprinting*, 2021. http://creativecommons.org/licenses/by-nc-nd/4.0/.

14. E. Garreta, R. Oria, C. Tarantino, M. Pla-Roca, P. Prado, F. Fernandez-Aviles, J. M. Campistol, J. Samitier and N. Montserrat, "Tissue engineering by decellularization and 3D bioprinting," *Materials*, no. 4, pp. 166-178, 2017.

15. Mironov, Vasiliy, T. Trusk, V. Kasyanov, S. Little, R. Swaja, and R. Markwald. "Biofabrication: a 21st century manufacturing paradigm." *Biofabrication*, vol. 1, no. 2, 022001, 2009.

16. N. Vermeulen, G. Haddow, T. Seymour, *et al*., "3D bioprinting: a socioethical view of bioprinting human organs and tissues," *Journal of Medical Ethics*, vol. 43, pp. 618-624, 2017.

17. D. E. Ingber, "Human organs-on-chips for disease modelling, drug development and personalized medicine," *Nature Reviews Genetics*, vol. 23, no. 8, pp. 467-491, 2022.

18. Y. Zhu, D. Joralmon, W. Shan, Y. Chen, J. Rong, H. Zhao, S. Xiao and X. Li, "3D printing biomimetic materials and structures for biomedical applications." *Bio-Design and Manufacturing*, vol. 4, pp. 405-428, 2021.

19. H. Tan, K. Yang, P. Wei, G. Zhang, D. Dimitriou, L. Xu, W. Huang and X. Luo, "A novel preoperative planning technique using a combination of CT angiography and three-dimensional printing for complex toe-to-hand reconstruction." *Journal of Reconstructive Microsurgery*, vol. 31, no. 05, pp. 369-377, 2015.

20. S. Kabene and S. Baadel, "Bioethics: a look at animal testing in medicine and cosmetics in the UK," *Journal of medical ethics and history of medicine*, vol. 12, 2019.

21. N. Picollet-D'hahan, A. Zuchowska, I. Lemeunier and S. L. Gac, "Multiorgan-on-a-chip: a systemic approach to model and decipher inter-organ communication, " *Trends in biotechnology*, vol. 39, no. 8, pp. 788-810, 2021.

22. D. Rana, H. Zreiqat, N. Benkirane-Jessel, A. Ramakrishna and M. Ramalingam. "Development of decellularized scaffolds for stem cell-driven tissue engineering,"*Journal of tissue engineering and regenerative medicine*, vol. 11, no. 4, pp. 942-965. 2017.

23. D.Y.C. Cheung, B. Duan and J.T. Butcher Essent, *3D Biofabrication Transl*, pp.

351-370, 2015.

24. Y. Dzenis, "Spinning continuous fibers for nanotechnology," *Science*, vol. 304, no. 5679, pp. 1917-1919, 2004.

25. G. A. Whitney, K. Jayaraman, J. E. Dennis and J. M. Mansour, "Scaffold-free cartilage subjected to frictional shear stress demonstrates damage by cracking and surface peeling," *Journal of tissue engineering and regenerative medicine*, vol. 11, no. 2, pp. 412-424, 2017.

26. S. N. Bhatia, D. E. Ingber, "Microfludic organ-on-chips," *Nat Biotechnol*, vol. 32, pp. 760-772, 2014.

27. S. V. Murphy, A. Skardal and A. Atala, " Evaluation of hydrogels for bio-printing applications," *Journal of Biomedical Materials Research Part A*, vol. 101 no. 1, pp. 272-284, 2012.

28. Y. Zhang, Y. Yu, A. Akkouch, A. Dababneh, F. Dolati and I. T. Ozbolat, "In vitro study of directly bioprinted perfusable vasculature conduits," *Biomaterials science*, vol. 3, no. 1, pp. 134-143, 2015.

29. R. J. Klebe, "Cytoscribing: a method for micropositioning cells and the construction of two-and three-dimensional synthetic tissues," *Experimental cell research*, vol. 179, no. 2, pp. 362-373, 1988.

30. A. Santoni, S. G. Gugliandolo, M. Sponchioni, D. Moscatelli and B. M. Colosimo, "3D bioprinting: current status and trends—a guide to the literature and industrial practice," *Bio-Design and Manufacturing*, vol. 5, no. 1, 14-42, 2022.

31. Y. S. Zhang, G. Haghiashtiani, T. Hübscher, D. J. Kelly, J. M. Lee, M. Lutolf, M. C. McAlpine, W. Y. Yeong, M. Zenobi-Wong and J. Malda, "3D extrusion bioprinting," *Nature Reviews Methods Primers*, vol.1, no. 1, p. 75, 2021.

32. S. Bashir, M. Hina, J. Iqbal, A. H. Rajpar, M. A. Mujtaba, N. A. Alghamdi, S. Wageh, K. Ramesh, and S. Ramesh, "Fundamental concepts of hydrogels: Synthesis, properties, and their applications," *Polymers*, vol. 12, no.11 p.2702, 2020.

33. C. L. Ventola, "Medical applications for 3D printing: current and projected uses," *Pharmacy and Therapeutics*, vol. 39, no. 10, p. 704, 2014.

34. I. T. Ozbolat, “Bioprinting scale-up tissue and organ constructs for transplantation,” *Trends Biotechnol*, vol. 33 no. 7, pp. 395-400, 2015.

35. H. Handral, S. Tay, W. Chan, D. Choudhury, “3D Printing of Cultured Meat Products,” *Critical Reviews in Food Science and Nutrition*, vol. 62 no. 1, pp. 272-281, 2020.

36. X. Guo, D. Wang, B. He, *et al.*, “3D Bioprinting of Cultured Meat: A Promising Avenue of Meat Production,” *Food Bioprocess Technol*, 2023.

37. K. Handral, H. H. Tay, S. W. Chan and D. Choudhury, "3D Printing of cultured meat products," *Critical Reviews in Food Science and Nutrition*, vol. 62 no. 1, pp. 272-281, 2022.

38. J. Gopinathan and I. Noh, "Recent trends in bioinks for 3D printing,"*Biomaterials research*, 22, 1-15, 2018.

39. A. Kirillova, B. Stanislav, A. Aydar and S. Gennady, "Bioethical and legal issues in 3D bioprinting," *International Journal of Bioprinting* vol. 6, no. 3 2020.

40. K. Loukelis, Z. A. Helal, A. G. Mikos and M. Chatzinikolaidou, "Nanocomposite bioprinting for tissue engineering applications," *Gels* 9, no. 2, p.103, 2023.

41. E. D. Ker, B. Chu, J. A. Phillippi, B. Gharaibeh, J. Huard, L. E. Weiss and P. G. Campbell, "Engineering spatial control of multiple differentiation fates within a stem cell population," *Biomaterials*, vol. 32, no. 13 pp. 3413-3422, 2011.

42. A. Arslan-Yildiz, R. E. Assal, P. Chen, S. Guven, F. Inci and U. Demirci, "Towards artificial tissue models: past, present, and future of 3D bioprinting" Biofabrication, vol. 8, no. 1, p. 014103, 2016.

43. S. **D**avide, "The top 15 Bioprinters", August 26th, 2015. https://3dprintingindustry.com/news/top-10-bioprinters-55699/

44. faCellitate,"What are the types of 3D bioprinting technologies?" https://facellitate.com/what-are-the-types-of-3d-bioprinting-technologies/

45. N. Ramirez, "Assessing 3D Printability of Bioinks," *University of Central Florida Honors Undergraduate Theses*, vol. 748, pp. 3-5, 2020.

46. A. Ovsianikov, M. Gruene, M. Pflaum, L. Koch, F. Maiorana, M. Wilhelmi, A. Haverich and B. Chichkov, “Laser printing of cells into 3D Scaffolds,” *Biofabrication*, vol. 2, p. 014104, 2010.

47. M. E. Hoque, Y. L. Chuan and I. Pashby, “Extrusion based rapid prototyping technique:an advanced platform for tissue engineering scaffold fabrication,” *Biopolymers*, vol. 97, pp. 83-93, 2012.

48. S. Anupama, "3D Bioprinting- Definition, Principle, Process, Types, Applications," 2023.

49. S. V. Murphy and A. Atala. "3D bioprinting of tissues and organs, " *Nature biotechnology*, vol. 32, no. 8, pp. 773-785, 2014.

50. M. R. Sankar, D. V. Krishna, "Engineered Regeneration," vol. 4, no. 4, pp. 396-410, 2023.

51. L. Ouyang, R. Yao, Y. Zhao and W. Sun, "Effect of bioink properties on printability and cell viability for 3D bioplotting of embryonic stem cells," *Biofabrication,* vol. 8, no. 3 (2016): 035020.

52. M. Janmaleki, J. Liu, M. Kamkar, M. Azarmanesh, U. Sundararaj and A. S. Nezhad, "Role of temperature on bio-printability of gelatin methacryloyl bioink in two-step cross-linking strategy for tissue engineering applications," *Biomedical Materials*, vol. 16, no. 1, p. 015021, 2020.

53. R. Polak, F. Sedlacek and K. Raz, "Determination of FDM printer settings with regard to geometrical accuracy," *In Proceedings of the 28th DAAAM international symposium*, pp. 0561-0566, 2017.

54. J. W. Haycock, "3D cell culture: a review of current approaches and techniques," *Humana Press,* 2011.

55. A. Tirella, A. Orsini, G. Vozzi and A. R. T. I. Ahluwalia, "A phase diagram for microfabrication of geometrically controlled hydrogel scaffolds," *Biofabrication,* vol. 1, no. 4, p. 045002, 2009.

56. S. Ramesh, O. L. Harrysson, P. K. Rao, A. Tamayol, D. R. Cormier, Y. Zhang and I. V. Rivero, "Extrusion bioprinting: Recent progress, challenges, and future opportunities," *Bioprinting*, vol. 21, p. e00116, 2021.

57. A. L. Rutz, P. L. Lewis and R. N. Shah, "Toward next-generation bioinks: tuning material properties pre-and post-printing to optimize cell viability," *MRS Bulletin*, vol. 42, no. 8, pp. 563-570, 2017.

58. A. Panwar and L. P. Tan, "Current status of bioinks for micro-extrusion-based 3D bioprinting," *Molecules*, vol. 21, no.6. p.685, 2016.

59. G. Gillespie, P. Prim, J. Copus, J. Fisher, A. G. Mikos, J. J. Yoo, A. Atala and S. J. Lee, "Assessment methodologies for extrusion-based bioink printability," *Biofabrication,* vol. 12, no. 2, p. 022003, 2020.

60. I. T. Ozbolat and M. Hospodiuk, "Current advances and future perspectives in extrusion-based bioprinting," Biomaterials, vol. 76, pp. 321-343, Jan. 2016. doi: 10.1016/j.biomaterials.2015.10.076.

61. V. I. Obama and H. Eagle, "Measurement of cell growth in tissue culture with a phenol reagent (Folin-Ciocalteau)," *Proceedings of the Society for Experimental Biology and Medicine*, vol. 91, no. 2, pp. 305-307, 1956.

62. B. Houwen, "The differential cell count," *Laboratory Hematology* , vol. 7, pp. 89-100, 2001.

63. W. Hu, "Dry weight and cell density of individual algal and cyanobacterial cells for algae research and development", *University of Missouri-Columbia*, 2014.

64. E. D′ Haese and H.J. Nelis, "Rapid detection of single cell bacteria as a novel approach in food microbiology," *Journal of AOAC International*, vol. 85, no. 4, pp. 979-983, 2002.

65. H. Y. Lan, P. Hutchinson, G. H. Tesch, W. Mu and R. C. Atkins, "A novel method of microwave treatment for detection of cytoplasmic and nuclear antigens by flow cytometry," *Journal of immunological methods*, vol. 190, no. 1, pp. 1-10, 1996.

66. W. J. Goh, S. Zou, C. K. Lee, Y. Ou, J. W. Wang, B. Czarny and G. Pastorin, "EXOPLEXs: chimeric drug delivery platform from the fusion of cell-derived nanovesicles and liposomes," *Biomacromolecules*, vol. 19, no. 1, pp. 22-30, 2018

67. C. Tapeinos, A. Marino, M. Battaglini, S. Migliorin, R. Brescia, A. Scarpellini, C. D. Fernández, M. Prato, F. Drago and G. Ciofani, "Stimuli-responsive lipid-based magnetic nanovectors increase apoptosis in glioblastoma cells through synergic intracellular hyperthermia and chemotherapy," *Nanoscale*, vol. 11, no. 1, pp. 72-88, 2019.

68. F. J. Gordillo, M. Goutx, F. L. Figueroa and F. X. Niell, "Effects of light intensity, CO 2 and nitrogen supply on lipid class composition of Dunaliella viridis," *Journal of applied phycology*, vol. 10, pp.135-144, 1998.

69. S. R. Joy and T. R. Anju, "Microalgal Biomass: Introduction and Production Methods" In: S. Thomas, M. House, D. Pasquini, C. J Chirayil, (eds) *Handbook of Biomass, Springer Singapore*, 2023.

70. B. Lv, Z. Liu, Y. Chen, S. Lan, J. Mao, Z. Gu, A. Wang, F. Yu, X. Zheng and H. E. Vasquez. "Effect of different colored LED lighting on the growth and pigment content of Isochrysis zhanjiangensis under laboratory conditions," *Journal of Marine Science and Engineering* vol. 10, no. 11 p. 1752, 2022.

71. S. Sebastian, P. W. Sanofi Roche, M. Hochschule, " Monitoring of Cell Culture Cell Engineering: Animal Cell Culture" vol. 9, no. 7, pp.185-221,

72. K.Alexandra, K. Gerulová, "Microalgae Harvesting: A Review," *Research Papers Faculty of Materials Science and Technology Slovak University of Technology*, vol. 27, no. 44, pp. 129-143, 2019.

73. H. Tan, S. Guo, N. D. Dinh, R. Luo, L. Jin and C.H. Chen, "Heterogeneous multi-compartmental hydrogel particles as synthetic cells for incompatible tandem reactions," *Nature Communications*, vol. 8, no. 1, p. 663, 2017.

74. J. Li, Y. Zhang, Y. Huang, B. Luo, L. Jing and D. Jing, "Noble-metal free plasmonic nanomaterials for enhanced photocatalytic applications—A review," *Nano Research*, vol. 15, no. 12, pp. 10268-10291, 2022.

75. K. Na, S. Shin, H. Lee, D. Shin, J. Baek, H. Kwak, M. Park, J. Shin and J. Hyun, "Effect of solution viscosity on retardation of cell sedimentation in DLP 3D printing of gelatin methacrylate/silk fibroin bioink," *Journal of Industrial and Engineering Chemistry,* vol. 61, pp. 340-347, 2018.

76. A. Trager, S. Naeimipour, M. Jury, R. Selegård and D. Aili, "Nanocellulose Reinforced Hyaluronan-Based Bioinks," *Biomacromolecules*, 2023.

77. J. Malda, J. Visser, F. P. Melchels, T. Jüngst, W. E. Hennink, W. J. Dhert, J. Groll and D. W. Hutmacher, "25th anniversary article: engineering hydrogels for biofabrication," *Advanced materials*, vol. 25, no. 36, pp. 5011-5028, 2013.

78 W. Fang, M. Yang, L. Wang, W. Li, M. Liu, Y. Jin, Y. Wang *et al*., "Hydrogels for 3D bioprinting in tissue engineering and regenerative medicine: Current progress and challenges," *International Journal of Bioprinting*, vol. 9, no. 5, 2023.

79. T. Gao, G. J. Gillispie, J. S. Copus, A. K. Pr, Y. J. Seol, A. Atala, J. J. Yoo and S. J. Lee, "Optimization of gelatin–alginate composite bioink printability using rheological parameters: A systematic approach," Biofabrication, vol. 10, no. 3, p. 034106, 2018.

80. L. Ouyang, R. Yao, Y. Zhao and W. Sun, "Effect of bioink properties on printability and cell viability for 3D bioplotting of embryonic stem cells," *Biofabrication*, vol. 8, p. 035020, 2016.

81. N. Paxton, W. Smolan, T. Bock, F. Melchels, J. Groll and T. Jungst, "Proposal to assess printability of bioinks for extrusion-based bioprinting and evaluation of rheological properties governing bioprintability," *Biofabrication*, vol. 9, p. 044107, 2017.

82. F. Xin and Q. Lyu, "A Review on Thermal Properties of Hydrogels for Electronic Devices Applications, *Gels*, vol. 9, no. 1, p. 7, 2022.

83. T. Ahlfeld, G. Cidonio, D. Kilian, S. Duin, A. R. Akkineni, J. I. Dawson, S. Yang, A. Lode, R. O. C. Oreffo and M. Gelinsky, "Development of a clay based bioink for 3D cell printing for skeletal application," *Biofabrication*, 9, no. 3, p. 034103, 2017.

84. K. A. Deo, K. A. Singh, C. W. Peak, D. L. Alge and A. K. Gaharwar, "Bioprinting 101: design, fabrication, and evaluation of cell-laden 3D bioprinted scaffolds," *Tissue Engineering Part A*, vol. 26. 5-6, pp. 318-338, 2020.

85. H. H. Tønnesen and J. Karlsen, "Alginate in drug delivery systems." *Drug*

development and industrial pharmacy, vol. 28, no. 6, pp. 621-630, 2002.

86. M. S. Hasnain, E. Jameel, B. Mohanta, A. K. Dhara, S. Alkahtani and A. K. Nayak, "Alginates: sources, structure, and properties," *In Alginates in drug delivery*, pp. 1-17. *Academic Press*, 2020.

87. J. Zeng, Z. Zeng, Z. Cheng, Y. Wang, X. Wang, B. Wang and W. Gap, "Cellulose nanofibrils manufactured by various methods with application as paper strength additives," *Scientific Reports*, vol. 11, no. 1, p. 11918, 2021.

88. Z. Cheng, R. Yang, X. Liu, X. Liu and H. Chen. "Green synthesis of bacterial cellulose via acetic acid pre-hydrolysis liquor of agricultural corn stalk used as carbon source." Bioresource technology 234 (2017): 8-14.

89. F. Li, E. Mascheroni and L. Piergiovanni, "The potential of nanocellulose in the packaging field: a review," *Packaging Technology and Science*, vol. 28, no. 6, 475-508, 2015.

90. A. H. Tayeb, E. Amini, S. Ghasemi and M. Tajvidi. "Cellulose nanomaterials—Binding properties and applications: A review," *Molecules*, 23, no. 10, p. 2684, 2018.

91. A. Zennifer, P. Senthilvelan, S. Sethuraman and D. Sundaramurthi. "Key advances of carboxymethyl cellulose in tissue engineering & 3D bioprinting applications," *Carbohydrate Polymers*, vol. 256, p. 117561, 2021.

92. M. I. H. Sohaimy and M. I. N. Isa, "Ionic conductivity and conduction mechanism studies on cellulose based solid polymer electrolytes doped with ammonium carbonate," *Polymer Bulletin*, vol. 74, pp. 1371-1386, 2017.

93. D. Therriault, S. R. White and J. A. Lewis, "Rheological behavior of fugitive organic inks for direct-write assembly," *Applied Rheology*, vol. 17, no. 1, p. 10112-1, 2007.

94. H. K. Lichtenthaler and C. Buschmann, "Chlorophylls and Carotenoids: Measurement and Characterization by UV-VIS Spectroscopy, *Current Protocols in Food Analytical Chemistry, no. 1, 2001*.

95. "Plants in Action: A resource for teachers and students of plant science", section 1.2.2, *Australian Society of Plant Scientists*, visited October 2023, https://www.asps.org.au/publications/plants-in-action

96. Beer-Lambert Law, *Edinburgh Instruments*, visited October 2023**.** https://www.edinst.com/us/blog/the-beer-lambert-law/

97. J. M. Parnis, K. B. Oldham, "Beyond the Beer–Lambert law: The dependence of absorbance on time in photochemistry" *Journal of Photochemistry and*

Photobiology A-chemistry, 267, 6-10, 2013.

98. T. J. Hinton, Q. Jallerat, R. N. Palchesko, J. H. Park, M. S. Grodzicki, H. J. Shue, M. H. Ramadan, A. R. Hudson, and A. W. Feinberg, "Three-dimensional printing of complex biological structures by freeform reversible embedding of suspended hydrogels," Sci. Adv., vol. 1, no. 9, Oct. 2015

99. S. Landerneau, L. Lemarié, C. Marquette, and E. Petiot, "Green 3D bioprinting of plant cells: A new scope for 3D bioprinting," *Bioprinting*, vol. 27, p. e00216, 2022.

100. S. M. Park, H. W. Kim, and H. J. Park, "Callus-based 3D printing for food exemplified with carrot tissues and its potential for innovative food production," *J. Food Eng.*, vol. 271, 2020.

101. K. Thakare, L. Jerpseth, Z. Pei, B. Tomlin, and H. Qin, "Three-Dimensional Printing of Hydrogel Filters Containing Algae Cells for Copper Removal From Contaminated Water," *J. Manuf. Sci. Eng. Trans. ASME*, vol. 143, no. 1, p. 022001, Jan. 2021.

102. T. Ahlfeld, M. Adolph, S. Kümmritz, J. Steingroewer, F. Krujatz, T. Bley, M. Gelinsky, and A. Lode, "Green bioprinting: extrusion-based fabrication of plant cell-laden biopolymer hydrogel scaffolds," *Biofabrication*, vol. 9, no. 1, p. 015028, 2017.

103. F. Krujatz, A. Lode, S. Brüggemeier, K. Schütz, J. Kramer, T. Bley, M. Gelinsky, and J. Weber, "Green bioprinting: viability and growth analysis of microalgae immobilized in 3D-plotted hydrogels versus suspension cultures," *Eng. Life Sci.*, vol. 15, pp. 678-688, 2015.

104. A. Lode, F. Krujatz, S. Brüggemeier, M. Quade, K. Schütz, S. Knaack, J. Weber, T. Bley, M. Gelinsky, S. Bruggemeier et al., "Green bioprinting: fabrication of photosynthetic algae-laden hydrogel scaffolds for biotechnological and medical applications," *Eng. Life Sci.*, vol. 15, pp. 177-183, 2015.

BIOGRAPHY OF THE AUTHOR

Olubusuyi Ayowole, known as Busuyi, was born on December 1, 1983, in Ilesa and is a native of Iperindo-Ijesa, Osun State, Nigeria. He graduated high school in 2001 from Ogedengbe School of Science, Ilesa, Nigeria, where he was recognized as the best essay writer at graduation. In 2003, Busuyi attended a Diploma course in Computer Technology at Obafemi Awolowo University, Ile-Ife. He entered the Federal University of Technology Akure (FUTA) for Mechanical Engineering in 2004 and graduated in December 2009 with a B.Eng, Second Class Upper Honours. Busuyi has pursued a career that blends his skills in music and engineering. He obtained his M.Sc. in Mechanical Engineering (concentration: Design and Production Engineering) from the University of Lagos (UNILAG) in January 2018. Seeking further competence and aiming to build an international career as a professional engineer, Busuyi enrolled in the M.S. program at the University of Maine in Spring 2022. After the Spring 2022 semester, he participated in the governorship election as the candidate of the Peoples Redemption Party in Osun State, Nigeria, in July 2022, competing alongside candidates from 14 other political parties. Busuyi is a candidate for the Master of Science degree in Mechanical Engineering from the University of Maine in August 2024.